Viscoelastic Polymer Flooding and Residual-Oil Desaturation: A Criteria-Screened Evidence Synthesis, Carbonate Injectivity Bounds, and Experimental Design

Imad A. Adel[a], Alvaro Hernandez[a], Emad W. Al-Shalabi[a,b], Waleed Alameri[a,b]

[a] *Chemical and Petroleum Engineering Department, Khalifa University of Science and Technology, Abu Dhabi, United Arab Emirates*
[b] *Research and Innovation Center on CO_2 and Hydrogen (RICH), Khalifa University of Science and Technology, Abu Dhabi, United Arab Emirates*

* *Manuscript in preparation for* ***Petroleum Science*** *(KeAi Publishing).*

Abstract

Published corefloods contradict one another on whether polymer viscoelasticity reduces residual oil saturation (S_{or}) beyond the viscous contribution. Whether test design structures the contradiction is tested with a criteria-screened evidence synthesis: 39 published studies were reduced through logged admission criteria to seven studies holding a matched-viscosity inelastic reference, yielding 49 elastic-versus-reference contrasts on one declared velocity and capillary-number basis. (1) The primary quantity is the paired within-study high-minus-low velocity difference across the four studies carrying both regimes: +0.047, +0.005, +0.024, and −0.037 saturation units. The mean is +0.010, and the paired interval at three degrees of freedom is [−0.046, +0.066]. The corpus does not resolve an independent velocity effect attributable to viscoelasticity. (2) Stage-level cells do not separate (+0.052 above 1 ft/D (0.3048 m/d), n = 15, against +0.059 at or below it, n = 17); five stages sit at the boundary; the ordering depends on their assignment. Every salinity-unconfounded tertiary increment of at least 0.10 saturation units lies at or above 1 ft/D; the signal localizes in glycerol-referenced floods of one laboratory lineage whose elastic stages ran 1.2–2.1 times more resistive in-core than their references there. (3) The corpus contains no matched-reference support for a secondary-mode elastic advantage. (4) Stage-wise salinity change and the endpoint relative-permeability convention (a 1.3–2.9-fold capillary-number bias) inflate compiled-curve scatter. Injectivity measurements in six carbonate reservoir cores place the apparent onset of increasing porous-medium resistance between at or below 0.93 ft/D (0.283 m/d) and 6.6–13.1 ft/D (2.01–3.99 m/d), history-dependent, absent to 88 ft/D (26.8 m/d) in one run; retention and permeability reduction are not excluded. At q/h = 10 m³/d per metre and φ = 0.23–0.31, that regime lies within roughly 2–24 m of an unfractured vertical injector (open above; the lowest onset is one-sided): a necessary condition for viscoelastic desaturation, not a demonstration of it. A minimum reporting checklist and a matched-reference carbonate experiment are specified.

Keywords: polymer flooding; viscoelasticity; residual oil saturation; capillary desaturation curve; polymer injectivity; carbonate reservoirs

1. Introduction

1.1 The contradiction and its stakes

Whether the elasticity of hydrolyzed-polyacrylamide (HPAM) solutions mobilizes capillary-trapped oil beyond the viscous contribution remains unresolved and bears directly on slug sizing and forecast incremental oil in chemical enhanced oil recovery. The affirmative case originates with the Daqing laboratory and field programme (Wang et al., 2000, 2001a), was given a mechanistic and mode-dependent interpretation by Huh and Pope (2008) using secondary-mode floods compiled from earlier theses (Wreath, 1989), and was reinforced by sandstone corefloods reporting large incremental desaturation. The skeptical case attributes the reported reductions to non-elastic channels such as adsorbed-polymer pore-throat narrowing (Sandengen et al., 2017), and questions whether the effect is workable at the low velocities of unfractured field wells (Seright and Wang, 2023). Four test-design channels recur across the contradictory reports and are screened for in this work: capillary end effects, unstable initial waterfloods, stage-to-stage salinity changes, and capillary numbers computed on inconsistent conventions. Critical reviews (Azad and Trivedi, 2019) document the contradiction without resolving it.

Polymer flooding is advancing into high-temperature, high-salinity carbonates, among them the single-well injectivity test and multi-well pilot design in a giant onshore Abu Dhabi limestone (Fabbri et al., 2021). There the economic case is built on sweep improvement, and any additional displacement-efficiency credit from viscoelasticity would materially change slug sizing and forecast incremental oil. Claiming that credit requires knowing whether the laboratory effect is real, under which conditions it appears, and whether those conditions exist at field velocities. The reviews have not settled this because they catalogue results without imposing a common admissibility standard: studies that differ simultaneously in reference fluid, injection mode, flow intensity, salinity history, and capillary-number convention are compared as if they tested the same hypothesis. In this work, the admissibility standard is imposed before comparison.

1.2 Prior art: existing desaturation quantifications

No new desaturation curve is introduced in this work. Curve-type quantifications already exist in two forms: the Deborah-number-based elastic desaturation model implemented in simulation by Qi et al. (2018), and the extensional-capillary-number (N_{ce}) correlation of Azad and Trivedi (2021), which compiles literature floods into an $S_{or}(N_{ce})$ trend and is additionally protected as a screening method by a United

States patent (Azad and Trivedi, 2023). The N_{ce} of Azad and Trivedi (2021) is adopted unchanged, as an existing tool, and the implementation is verified independently against their published values (Section 2.4).

1.3 Contribution

The contribution of this work is the screen, not the curve. No published study was identified that (i) imposes an explicit admission criterion (a matched-viscosity inelastic reference within the same study) across the contradictory corpus with a documented exclusion log; (ii) re-expresses every admitted flood on one declared velocity and capillary-number convention with per-value provenance; (iii) classifies the resulting elastic-versus-reference contrasts by the two test-design factors most often invoked qualitatively, injection mode and flow intensity, and tests whether the contradiction is thereby structured; and (iv) quantifies two further conventions-and-confounders channels (endpoint versus saturation-dependent water relative permeability, and stage-to-stage salinity change) as measurable contributors to capillary-desaturation-curve scatter. Under the primary velocity-only classification, the tertiary stage-level cells do not separate (+0.052 against +0.059 saturation units); an ordering appears only when the five boundary stages are reassigned or under the superseded velocity-or-pressure-gradient classifier (Section 3.3). The structure that survives the screen is conditional: every matched-reference increment of at least 0.10 saturation units in the salinity-unconfounded tertiary set lies at 1 ft/D (0.3048 m/d) or above, and the corpus is too small and too clustered to resolve a study-level velocity effect. The matched-reference record additionally contains no support for the frequently asserted secondary-mode advantage (Section 3.4).

2. Materials and methods

2.1 Source screening and evidence tiers

Thirty-nine published studies were inventoried (Appendix A lists the admitted studies; the full inventory is tabulated in the supplementary dataset). Five same-study merges reduced these to 34 evidence units (Appendix B); 15 were excluded with logged reasons (Appendix B), leaving 19 viscoelastic coreflood sources, of which seven were Admitted and 12 Supportive (Fig. 1). The comparison-level mapping is tabulated in supplementary Table S5. The corpus was assembled through a literature review of the published reviews of the contradiction, their reference lists, and the primary studies cited there. It was then extended by a reproducible search update over 2023–2026 across Crossref, OpenAlex, and Semantic Scholar, with declared strings, screening rules, and stated limitations recorded in the supplementary search log. The pre-2023 seed corpus is a review-derived sample assembled without a declared retrieval protocol; what is offered as reproducible is the admission screen and the search update, not the retrieval, and the update bounds the corpus at the stated cutoff rather than establishing completeness.

Sources were assigned to three tiers. Admitted: studies reporting endpoint saturations for a viscoelastic stage and a matched-viscosity inelastic reference (glycerol, xanthan, scleroglucan, or low-molecular-weight polymer at matched apparent viscosity or matched pressure gradient), with extractable velocity or pressure-gradient information; the reference criterion is applied at the study level, and the per-comparison in-core-reference status and injection order are carried in the dataset (Section 3.3). Supportive: studies missing one element (no inelastic reference, recovery-basis saturations, or unreported interfacial tension or geometry); these inform interpretation but never enter the quantitative comparisons. Excluded: units from which no numerically extractable quantity bearing on the question can be recovered, and reviews, theory, simulation, rheology-only, and field-only studies, recorded with reasons in Appendix B.

Seven studies were admitted under the matched-reference screen (Ehrenfried, 2013; Vermolen et al., 2014; Clarke et al., 2016; Qi et al., 2017; Erincik et al., 2018; Jin et al., 2020; Irfan et al., 2021). Cottin et al. (2014) were retained as Supportive mode-contrast evidence because the secondary and tertiary floods were referenced against water rather than a matched inelastic fluid. The glycerol-reference caveat is stated once in Section 2.8 and cross-referenced wherever glycerol anchors a comparison.

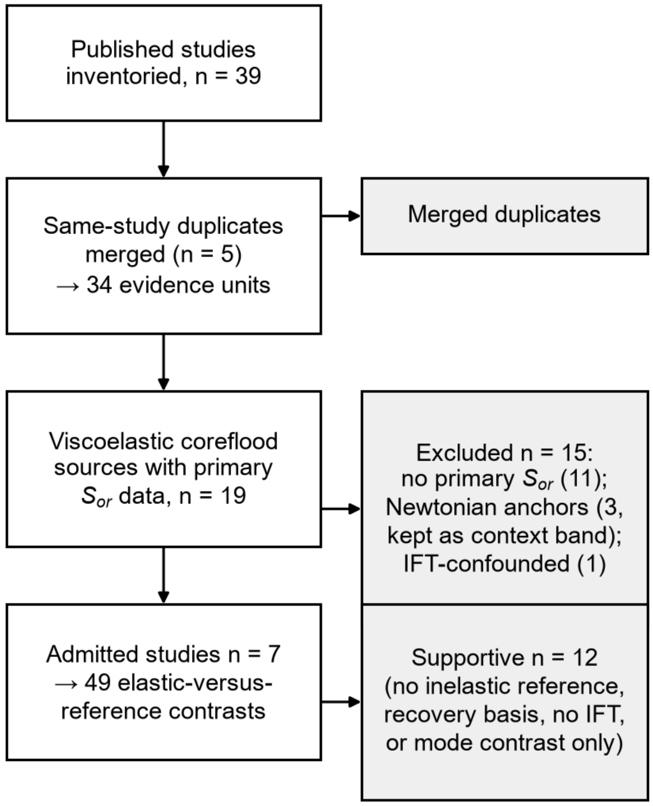

Fig. 1. Source-screening flow: 39 published studies (including the six 2023–2026 search-update studies; supplementary §S3), same-study merges, logged exclusions, and the resulting tiers (seven Admitted studies; 12 Supportive units; 15 Excluded with reasons in Appendix B). The Supportive tier includes one study retained specifically for secondary-versus-tertiary mode contrast without a matched inelastic reference.

Laboratory lineage is disclosed as an explicit dataset column because it bounds independence: Qi, Erincik, Jin, Ehrenfried and Koh share the UT Austin ecosystem (overlapping protocols, polymers, and outcrop cores), against Vermolen et al. (2014, Shell), Clarke et al. (2016, Schlumberger), Irfan et al. (2021, UTP), Cottin et al. (2014, TotalEnergies), and the Daqing study. Four of the seven admitted studies are one lineage, and a fifth study of the same lineage (Koh) sits in the Supportive tier; the statistical treatment of Section 2.7 exists because of this.

2.2 Extracted variables and provenance

For every flood and rate step the following were extracted: rock type and wettability, permeability, porosity, oil viscosity, fluid type and rheological descriptors (bulk viscosity, relaxation time, Deborah number where reported), endpoint saturations before and after the stage, velocity with its declared basis (interstitial frontal advance versus Darcy flux), pressure gradient, interfacial tension, end-effect mitigation, and injection mode. Each value carries a basis tag: reported (printed in the source), digitized (read from a figure or carried from a secondary tabulation), or estimated (stated assumption). Where a source is internally inconsistent, the per-experiment table value is used and the discrepancy is flagged in the dataset. One example is the Ehrenfried Bentheimer 11-Y summary table, whose stage recovery disagrees with its own oil-recovery table. The Clarke comparison is constructed against its low-elasticity 3130S reference (endpoint saturations 0.42 and 0.32, digitized via Azad and Trivedi (2021)); the waterflood-referenced value that circulates in compilations (0.13) overstates the elastic-versus-reference increment and is not used.

2.3 Velocity basis and capillary-number conventions

Reported velocities were converted to a single declared basis, interstitial velocity (frontal advance). The primary capillary number follows the microscopic convention, in the classification surveyed by Guo et al. (2022):

(1)

where v_i is interstitial velocity, μ_{app} the apparent displacing-phase viscosity, and σ the oil–water interfacial tension. Because several admitted studies report pressure gradients more reliably than rates, a secondary Brownell–Katz-type convention is carried in parallel, as used by Erincik et al. (2018) and Ehrenfried (2013):

(2)

Both numbers are tabulated for every stage; no point is plotted on a convention different from its neighbours. Two velocity bases appear in this work: the interstitial basis of Eq. 1, Eq. 2 and Eq. 5, and the superficial (Darcy) flux $u = \varphi v_i$ on which the shear-rate coefficient of Eq. 3 and the radial bound of Eq. 7 are defined; every reported value states its basis.

2.4 Extensional capillary number (existing tool, verified implementation)

The extensional capillary number replaces the bulk shear viscosity in Eq. 1 with a pore-scale apparent viscosity that includes a strain-hardening term (Azad and Trivedi, 2021). The in-situ shear rate, pore-scale apparent viscosity, and N_{ce} are computed as follows, with the shear rate evaluated on each source's reported velocity, the convention on which the published cases reproduce (supplementary §S1):

(3)

(4)

(5)

with C = 6, α = 2, and β = 0.01 as specified by Azad and Trivedi (2021); the 0.75 prefactor on the strain-hardening term is likewise carried unchanged, λ is the shear-model time constant and τext the extensional relaxation time. The implementation reproduces the source's tabulated pore-scale viscosities to better than 0.4% on each source's own velocity-reporting convention (superficial flux for Darcy-reporting sources, interstitial for frontal-advance reporting); the verification table, the worked example, and the recorded source-internal discrepancies are given in supplementary §S1. The patent variant (Azad and Trivedi, 2023) publishes slightly different constants. No claim is made to the N_{ce} concept or correlation; both are cited as prior art.

2.5 Normalization and relative-permeability sensitivity

Capillary numbers built on the aqueous-phase flux require k_{rw}. Most sources use the endpoint value; during desaturation the saturation-dependent value applies. The error is bounded with a Corey form, with S the water saturation and the error factor evaluating Eq. 6 at the pre- and post-stage saturations,

(6)

using n_w = 2.7–3.2 (the range fitted by Koh et al. (2018) for comparable systems) and Swr = 0.15 where unreported. For admitted tertiary stages with $\Delta S_{or} \geq 0.05$ the endpoint convention overstates k_{rw} (and hence flux-based capillary numbers) by a factor of 1.3–2.9 (n_w = 2.7–3.2); the largest swing in the corpus, a Supportive-tier stage, reaches an order of magnitude and enters no quantitative claim. This is a quantified, direction-known contributor to apparent scatter when literature points are co-plotted (Section 3.5).

2.6 Flow-intensity classification and its verification

Each comparison is classified on interstitial velocity alone: high-intensity above 1 ft/D (0.3048 m/d), low-intensity at or below it, applied as a strict inequality. The velocity term reflects the onset range repeatedly reported for elastic flow resistance in dilute HPAM. An earlier classification admitted a pressure-gradient disjunct of at least 10 psi/ft (226.2 kPa/m); that disjunct is retained only as a labelled sensitivity (supplementary Table S2, Fig. S2), because the pressure gradient is in part a response to the elastic resistance under test and is therefore partly endogenous to the contrast it classifies.

Five of the 32 tertiary salinity-unconfounded comparisons lie at exactly 1.0 ft/D: four Erincik low-salinity stages, injected at that nominal set-point by design, and the Clarke comparison, whose source reports its velocity as approximately 1 ft/D, so its cell assignment is not determinable from the published record. Both boundary treatments are reported in Section 3.3. The velocity cut is also regrouped at 0.5 and 2 ft/D (0.1524 and 0.6096 m/d; Fig. 4). Field relevance is bounded with the radial velocity around an unfractured vertical injector,

(7)

which gives the radius r^* inside which a given interstitial onset velocity is exceeded at porosity φ (Section 4.2). This is a conservative single-layer bound; fractures, thin high-flux layers and horizontal-well geometries extend it (Azad and Seright, 2025).

2.7 Statistical treatment: comparisons are not independent

The 49 comparisons are not mutually independent: rate steps on one core are serially correlated, in-core contrasts are chained (each elastic stage begins at its reference's endpoint), and studies contribute unequally. Three studies supply 35 of the 49 comparisons (Erincik 12, Ehrenfried 12, Jin 11), with Erincik alone supplying 18 admitted stages. In effect the 49 contrasts behave as roughly seven independent experiments, and every claim is tested at that level. Three guards are therefore applied. First, all cell means are reported at both the stage level and the study level (the mean of study means), including for the reference-grade split of Table 4. Second, uncertainty on the high-low intensity contrast is estimated with a study-resampling bootstrap that resamples studies, not stages, with replacement (10,000 draws with random seed 20260731; resamples in which either cell is empty are discarded and the effective count is reported; percentile intervals at six clusters are approximate and are labelled as such). A study-resampled interval for the paired estimator is not derived, because four clusters admit only 35 distinct resample combinations and cannot support a calibrated percentile interval; the paired inference rests on the t interval and the leave-one-out table. Third, a leave-one-study-out table shows the sensitivity of every cell to each study. The effective sample size for inference is the number of studies, not the number of stages.

2.8 Reference grading and capillary-number matching

Not all inelastic references are equal. Grade A references hold their viscosity in the porous medium (xanthan, scleroglucan, matched low-elasticity polymers such as Flopaam 3130S or 3230S or low-molecular-weight HPAM); Grade B is glycerol, whose viscosity is strongly temperature- and dilution-sensitive and which, being Newtonian, does not shear-thin in situ. Bulk matching therefore does not establish in-situ matching, and the direction of the resulting in-core viscosity offset is velocity-dependent and takes both signs across the corpus (Section 3.3); this is the single full statement of the glycerol-reference caveat, cross-referenced hereafter. Separately, every comparison carries ΔN_c, the log10 offset between the capillary number of the elastic stage and that of its own reference (pressure-gradient basis (Eq. 2) where both are reported, velocity basis otherwise). Matched-Δp designs are assigned $\Delta N_c = 0$ on the gradient basis by construction; design-matched comparisons (same core, same rate, same interfacial tension) are likewise carried at $\Delta N_c = 0$ with the convention recorded in the dataset; and for cross-core-referenced stages ΔN_c is computed against the cross-core control. Comparisons in which the elastic stage exceeded its reference by more than 0.5 log10 units are flagged, because part of any increment there can be ordinary capillary desaturation at an N_c not applied during the reference stage; results are reported for the full set and for the N_c-matched subset.

The domain-resolved assessment of comparator matching, core pairing, salinity control, sequence, throughput, saturation measurement, reference reuse and data provenance is given in Table B.1.

2.9 New carbonate injectivity measurements: provenance and basis

Six injectivity corefloods on carbonate reservoir cores are reported for the first time in this work (results in Section 3.6, Fig. 6; interpretation and the designed experiment in Section 4.4). Five of the six series carry tabulated native data (basis tags per point in the supplementary dataset); the single-phase test is digitized from figures and a summary table. Core preparation for CF-1 proceeded by primol drainage to Swi, primol displacement by crude-oil injection, oil-permeability measurement, aging at 90 °C for two weeks, glycerol/brine (80:20) forced imbibition to S_{or}, a brine flush, and water-permeability measurement at S_{or}; CF-2 reached Swi by porous-plate desaturation, and after aging, brine flooding fell short of a stabilized residual, so glycerol/brine was injected to further reduce the saturation before the final brine flush. Polymer solutions were prepared in the make-up brine without pre-shearing and filtered at 1.2 µm (CF-1, CF-3, BU73-4) or 3 µm (CF-2, BU464-6B): SAV10 powder and the Kemira polymer at 1,000 ppm, the SAV10 emulsion at 800 ppm. The brines were formation water at 243,000 ppm (CF-1, BU-86, BU73-4) and 193,500 ppm (BU464-6B) and seawater at 42,500 ppm (CF-2), at 50 °C except BU464-6B at 60 °C.

Resistance-factor tests began from a stabilized brine baseline; polymer was injected at stepped rates (0.05–7 cm³/min; per-test grids in the supplementary dataset) to pressure stabilization at each rate, and the resistance factor is the ratio of stabilized polymer to brine pressure drops at equal rate against the same-saturation baseline of the same core. For CF-1 and CF-2 the baseline was measured over 1–5 cm³/min and extrapolated linearly to lower rates, so resistance factors below approximately 13 ft/D (3.96 m/d) divide by an extrapolated denominator; two CF-1 points below 0.4 ft/D (0.122 m/d) (extrapolated brine pressure drops under 0.06 psi) are excluded, as are two CF-2 points at 0.69 and 1.37 ft/D (0.210 and 0.418 m/d) without pressure stabilization, attributed to low-rate plugging; for BU73-4 the baseline was measured across the full rate range. The CF-1 brine viscosity is ambiguous in the underlying measurements: 1.00 cP at 50 °C in the permeability determination against 1.08 cP in the fluid characterization, which would raise the computed brine permeability from 66 to 71.7 md; 66 md is carried, and the 41-cp conversion of Section 3.6 uses the 1.08-cP value. BU464-6B was flooded in three sequential runs; the plotted series is run 1, and the repeat runs returned resistance factors of 9 and 3 near 1 ft/D (0.3048 m/d) as the brine permeability at S_{or} fell from 116 to 51 to 27 md (0.114, 0.0503 and 0.0266 µm²). Core dimensions are reported for four cores (58.8 × 38.4, 76.24 × 37.63, 70.36 × 38.1, and 76.12 × 37.77 mm); for the remaining two only the diameters are recoverable from the velocity–rate mapping (approximately 37.4 and 38.3 mm, derived), and the interstitial-velocity back-calculation of Section 3.6 uses the reported diameters; for the two derived diameters no independent check exists, since they come from the same velocity-rate mapping they are used to confirm. No repeat measurements beyond the stated runs were made and no uncertainty is plotted.

3. Results

3.1 The contradiction on the conventional basis

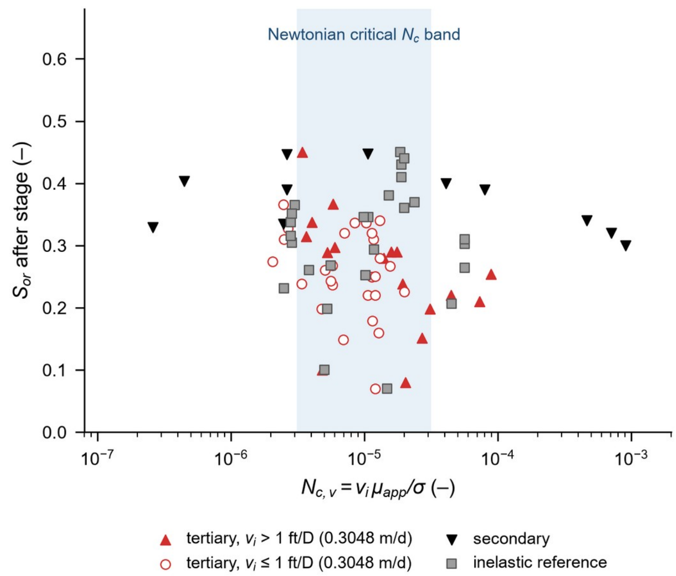

Fig. 2. Admitted floods on the conventional capillary-number basis (Eq. 1). Filled red triangles: tertiary stages above 1 ft/D (0.3048 m/d); open red circles: tertiary stages at or below it; black triangles: secondary stages; grey squares: inelastic reference stages. Shaded band: Newtonian critical range of Chatzis and Morrow (1984), re-expressed on the interstitial basis of Eq. 1 through their relative-permeability bridge (k_{rw} at residual 0.032–0.410) at their median porosity of 0.21 (conversion recorded in the supplementary dataset); the Abrams (1975) group carries a per-pair viscosity ratio and a saturation-change velocity basis and is therefore not re-expressible onto Eq. 1 as a single band (Section 3.1). Stages at indistinguishable $N_{c,v}$ report anywhere from zero to 0.21 saturation units of incremental desaturation.

Plotted on the single conventional basis, the admitted floods reproduce the contradiction as the literature presents it: at overlapping values of $N_{c,v}$ the recorded incremental desaturation spans zero to 0.21 saturation units (Fig. 2), and part of the admitted set lies within the re-expressed Newtonian critical range, where rate response alone can move S_{or}. The conventional capillary number therefore provides no discrimination among the admitted floods, consistent with the motivation of both the Deborah-number (Qi et al., 2018) and extensional (Azad and Trivedi, 2021) reformulations.

3.2 The extensional basis

On the N_{ce} basis the admitted stages are replotted against the published correlation (Fig. S1). The replot carries each stage on the source's own velocity-reporting convention (superficial flux for Darcy-reporting sources, interstitial for frontal-advance-reporting sources; basis tagged per value in the supplementary dataset), matching the construction of the published correlation. The reproduction verifies implementation consistency only: it does not validate the physical model, and no objective metric of improved ordering is computed here. The residual scatter is not random: the same stage can move across the trend depending on injection mode, flow-intensity regime and salinity history. That behaviour motivates the classification that follows.

3.3 Mode and flow intensity: stage-level structure and study-level inference

Stage-level cells (Table 1) are reported as descriptive context; the paired within-study contrast (Fig. 3; Table 2) is the primary quantity, and the classification sensitivity (Fig. 4; supplementary Table S2) bounds both.

Table 1. Stage-level elastic-versus-reference ΔS_{or} by injection mode and velocity regime. Upper panel: all 49 admitted comparisons (salinity-confounded stages included). Lower panel: tertiary comparisons with salinity-confounded stages excluded. These are the cells quoted in the text. High: v_i > 1 ft/D (0.3048 m/d), strict; positive means the elastic fluid desaturated further than its matched inelastic reference.

Mode	Intensity	n	Mean ΔSor (s.u.)	Min	Max
secondary	high	6	0.015	−0.078	0.100
secondary	low	5	−0.038	−0.109	0.008
tertiary	high	17	0.062	0.000	0.210
tertiary	low	21	0.070	0.000	0.150

At the stage level the cells do not separate in the expected direction (Fig. 4; Table 1): within unconfounded tertiary comparisons classified on interstitial velocity alone, the high cell averages +0.052 s.u. (n = 15) against +0.059 at or below the 1 ft/D (0.3048 m/d) cut (n = 17). Every increment of at least 0.10 s.u. in this subset lies at 1 ft/D or above, five of the eight at exactly the boundary. The ΔN_c-matched subset reproduces the absence of separation (+0.065 against +0.061, n = 6 and 10), so restricting to capillary-number-matched pairs does not restore an ordering.

Five of the 32 comparisons lie at exactly 1.0 ft/D: four Erincik low-salinity stages injected at that nominal set-point, and the single Clarke comparison at exactly 0.10 s.u. Assigning them to the high cell returns +0.068 (n = 20) against +0.036 (n = 12), so the stage-level ordering is a property of the boundary treatment as much as of the floods; it is reported as a descriptive statistic on that basis.

Under the superseded velocity-or-pressure-gradient classifier the cells did separate (+0.061 against +0.042); that classifier is retained only as a labelled sensitivity (supplementary Table S2, Fig. S2).

Two structural features of the contrasts bound this reading. In-core contrasts are chained: each elastic stage starts from its reference's endpoint, so the recorded contrast is the elastic increment from a saturation the reference already set. Injection order is also not constant across studies. In Jin coreflood 1 the elastic stage preceded its reference, is credited +0.110, and the glycerol stage injected after it removed a further 0.168 (0.238 to 0.070). Four Jin comparisons (J3, J6, J7, J11) carry no inelastic stage in their own cores and are admitted on the study-level reference, whereas the analogous Ehrenfried stages form no contrasts; the dataset flags both features per comparison, and the paired estimator moves within +0.004 to +0.015 under the corresponding re-screenings.

Table 2. Study-level cell means (tertiary, salinity-confounded stages excluded). The effective sample for inference is studies, not stages. Cells are velocity-only (high: v_i > 1 ft/D (0.3048 m/d)).

Study	Lineage	High: n / mean ΔSor	Low: n / mean ΔSor
CLARKE16	Schlumberger	–	1 / 0.100
EHREN13	UT Austin	5 / 0.018	1 / 0.055
ERIN18	UT Austin	2 / 0.125	4 / 0.120
IRFAN21	UTP	1 / 0.011	–
JIN20	UT Austin	3 / 0.067	8 / 0.043
QI17	UT Austin	4 / 0.057	3 / 0.010

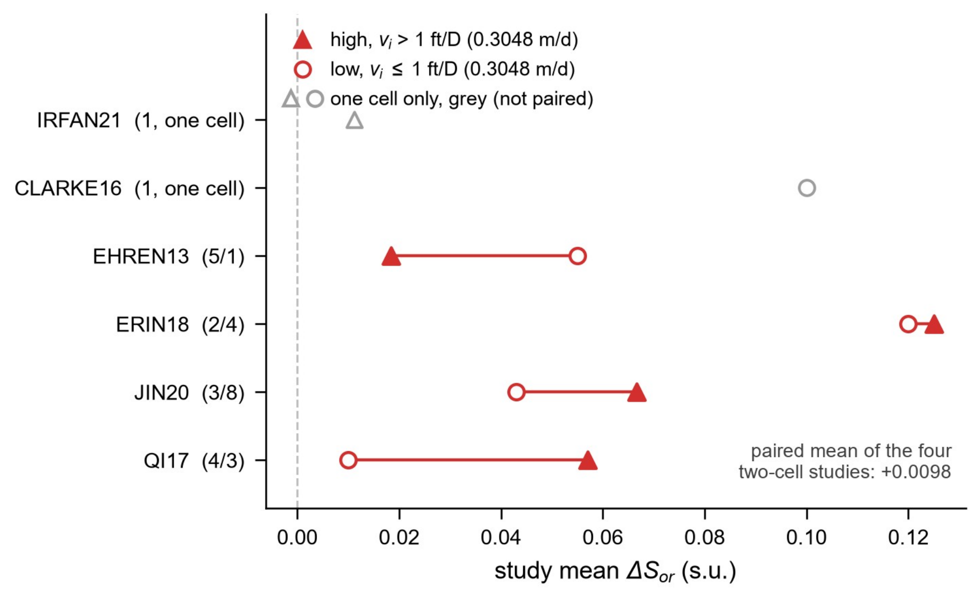

Fig. 3. Paired within-study elastic-versus-reference contrasts under the velocity-only classification. Filled triangles are the study mean ΔS_{or} above 1 ft/D (0.3048 m/d) interstitial velocity, open circles the mean at or below it, and the bar spans the paired difference; the counts in parentheses are the numbers of stages in the high and low cells. Grey symbols mark the two studies that carry only one cell and therefore form no paired difference. Each bar is one laboratory compared against itself at two flow rates. The unweighted mean of the four paired studies is +0.0098 saturation units; the paired t interval at three degrees of freedom is [−0.046, +0.066].

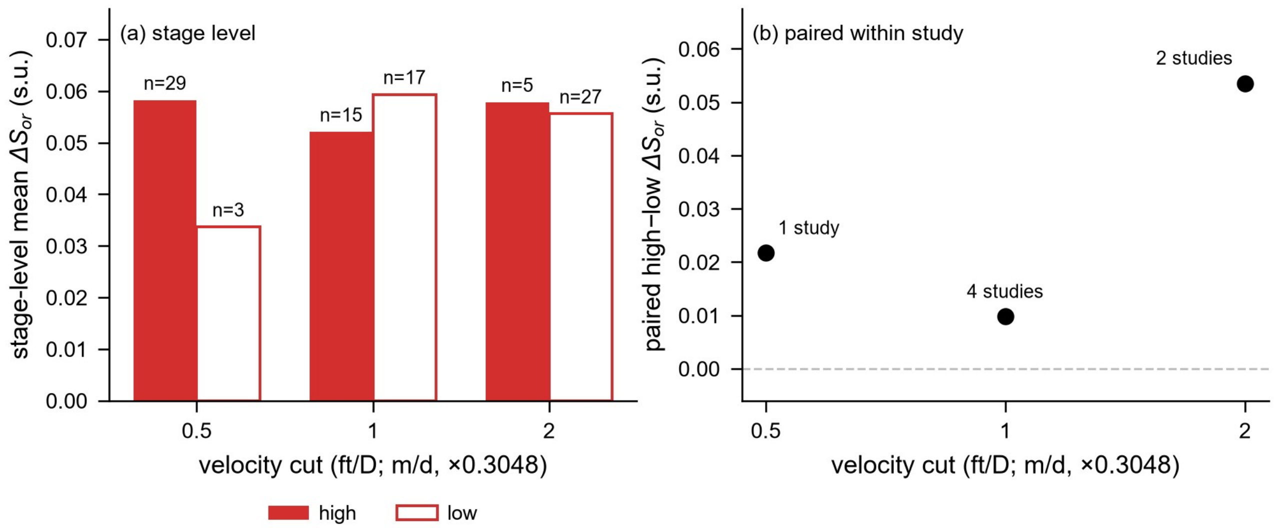

Fig. 4. Descriptive sensitivity of the velocity classification to the position of the cut-off. (a) Stage-level mean ΔS_{or} in the high and low cells at cut-offs of 0.5, 1 and 2 ft/D (0.1524, 0.3048 and 0.6096 m/d), with stage counts above each bar. (b) Unweighted mean paired within-study difference at the same cut-offs, annotated with the number of studies carrying both cells: one at 0.5 ft/D, four at 1 ft/D and two at 2 ft/D. The points carry no connecting line because the three cut-offs rest on different, partly non-overlapping study sets; the panel is a descriptive threshold-sensitivity analysis, not a physical threshold-response curve.

Four of the six tertiary studies (QI17, ERIN18, JIN20, EHREN13) carry both velocity cells (Fig. 3); the within-study difference holds laboratory, protocol, fluid systems and measurement practice fixed. The differences are +0.047, +0.005, +0.024 and −0.037 saturation units, and their unweighted mean is +0.010. Three are positive, one negative; the four span 0.084 saturation units. Removing any single study moves the mean within −0.003 to +0.025, and the sign reverses only when QI17 is removed. The paired t interval at three degrees of freedom is [−0.046, +0.066], which does not constrain the effect at four studies. CLARKE16 supplies only a low cell and IRFAN21 only a high cell, so neither enters the paired estimator, which is therefore independent of the Clarke ΔS_{or} value. The paired estimator is reported as primary because it is the only quantity that does not compare across laboratories. Under the inclusive boundary rule ERIN18 loses its low cell and leaves the estimator entirely, so the +0.011 obtained across the three remaining studies is the strict-rule leave-Erincik-out value rather than a perturbation of the four-study mean; the two figures rest on different study sets and are not comparable. The stage-level difference reverses from −0.007 to +0.032 under the same boundary change. The unpaired statistics that follow mix one-sided studies into the contrast and are retained as confounded sensitivities.

The interpretation is additionally constrained by the domain-resolved assessment in Table B.1, particularly cross-core comparator designs, shared references, unequal throughput and incomplete uncertainty reporting.

IRFAN21 contributes a single high-velocity comparison, and its admitted increment rests on 0.7 mL of recovered oil against a 62.33-mL pore volume, that is $\Delta S_{or} = 0.011$. The source does not report the collection-system accuracy or repeatability, so the significance of this increment cannot be established from the published record; its printed 3.27% figure is a remaining-oil basis, and the saturation-unit value is used here. It is retained at face value and flagged in the domain-resolved assessment rather than adjusted.

The unpaired study comparison (Table 2) likewise shows no separation: the mean of study means is +0.056 (high, five studies) against +0.066 (low, five studies), and a study-clustered bootstrap (approximate with six studies; seed 20260731; 9,999 of 10,000 effective resamples) places the stage-level high-low difference at −0.007 with a 95% percentile interval of [−0.063, +0.023]; 0.58 of effective resamples fall at or below zero. Leave-one-study-out (Table 3) moves the stage-level difference between −0.025 and +0.009; it reaches approximate zero only when Erincik, the study holding the four boundary stages, is removed. Four of the seven admitted studies are one laboratory lineage, and a fifth study of that lineage sits in the Supportive tier. Vermolen et al. (2014) contribute five secondary-mode comparisons and no tertiary comparison, and therefore do not appear in Tables 3 and 4. The defensible statement is therefore conditional, not universal: within the salinity-unconfounded tertiary set, every matched-reference elastic increment of at least 0.10 saturation units lies at an interstitial velocity of 1 ft/D (0.3048 m/d) or above, five of the eight at exactly the boundary velocity (across all 49 contrasts, thirteen increments reach 0.10 s.u., eight of them at the boundary), and the corpus is too small and too clustered for a velocity effect to be resolved at the study level.

Table 3. Leave-one-study-out sensitivity (tertiary, unconfounded): high/low cell means and their difference after dropping each study.

Dropped study	n high	Mean high	n low	Mean low	Difference
QI17	11	0.050	14	0.070	−0.020
ERIN18	13	0.041	13	0.041	+0.000
JIN20	12	0.048	9	0.074	−0.025
CLARKE16	15	0.052	16	0.057	−0.005
IRFAN21	14	0.055	17	0.059	−0.004
EHREN13	10	0.069	16	0.060	+0.009

Table 4. Reference-grade split (Grade A: xanthan, scleroglucan, matched low-elasticity polymers; Grade B: glycerol).

Subset	Cell	n	Mean ΔSor
Tertiary, unconfounded, Grade A	high	1	0.011
Tertiary, unconfounded, Grade A	low	5	0.048
Secondary, Grade A references	all	7	0.011
Secondary, Grade B (glycerol)	all	4	-0.044

The reference-grade split (Table 4) adds a further caveat: the large tertiary increments are glycerol-referenced (Erincik, Qi, Ehrenfried), while the six Grade-A-referenced tertiary comparisons divide under the velocity-only classification into one above 1 ft/D (0.3048 m/d) (+0.011) and five at or below it (mean +0.048, dominated by the single Clarke pair). The direction of the glycerol in-situ offset cannot be assigned a single sign, and where it is recoverable from stage-wise pressure gradients and velocities it runs against the elastic stages: the in-core resistance ratio of the elastic stage to its same-core glycerol reference spans 1.16–2.11 across the six Erincik pairs, so those elastic stages ran more resistive in-core, and the k_{rw} correction raises the ratio further. The same ratio spans 0.44–5.0 across Qi and 1.00–1.07 across Jin (∇p/v basis, Appendix A velocities and gradients). Part of the large glycerol-referenced increments can therefore be ordinary viscous displacement at an unmatched in-situ viscosity. The reference fluid is an uncontrolled design variable in the corpus; any velocity contrast in the corpus rests on Grade-B referencing, and no conclusion is drawn from the Grade-A subset with one comparison above the boundary.

Under the superseded classifier the high/low ordering is preserved when the cut is moved by a factor of two in either direction, because the pressure-gradient disjunct holds most high-gradient stages in the high cell at every cut; under the primary velocity-only classification there is no ordering to preserve (Fig. 4; the stage-level difference at the 1 ft/D cut is −0.007). Only the Clarke stage changes cells under the superseded classifier, whereas five comparisons sit at the boundary under the primary rule (Section 2.6). At the 0.5 ft/D (0.1524 m/d) cut the low cell retains only two comparisons, so that row bounds rather than verifies either classifier.

3.4 No matched-reference support for a secondary-mode advantage

The most cited mode evidence compares polymer against water: Huh and Pope's secondary Antolini floods (Huh and Pope, 2008), the Cottin et al. (2014) reservoir-core program, and the Daqing relative-permeability pairs (Wang et al., 2001a). Sweep efficiency and displacement history are therefore confounded with elasticity. In the only study that ran secondary elastic floods against secondary inelastic references on cores from the same outcrop blocks (Ehrenfried, 2013), the elastic floods did not reach lower endpoint saturations than their references. Across the two studies with matched secondary comparisons (Ehrenfried, 2013; Vermolen et al., 2014), the eleven comparisons average +0.011 s.u. against Grade-A references (n = 7) and −0.044 against glycerol (n = 4). At the study level the Grade-A mean reverses sign (−0.006 across two studies: Vermolen +0.034 over five comparisons resting on one cross-core control, Ehrenfried −0.046 over two comparisons sharing one xanthan reference), and the glycerol set is a single study; the eleven comparisons rest on five distinct reference floods, so the stated n overstates the independent information. Excluding the three Vermolen rate-bump stages, whose additional recovery the source attributes to the rate increase, the Grade-A stage mean is −0.023 (n = 4); netting the two bump increments against their cross-core control (which itself removed 0.010) gives +0.060 and +0.090 in place of +0.070 and +0.100. Had the Ehrenfried chapter-summary table been used instead of the per-experiment table (Section 2.2), the Bentheimer 11-Y secondary contrast would be −0.047 rather than −0.078, moving the glycerol mean to −0.037. Reference grade and intensity are strongly associated across these eleven comparisons: five of the seven Grade-A comparisons lie above 1 ft/D (0.3048 m/d) and three of the four glycerol-referenced ones at or below it. The grade and intensity readings are therefore only partly separable in this subset. The deficits concentrate in the glycerol-referenced pairs, and for Bentheimer 11-Y the source reports the mechanism directly: the glycerin stage ran 2.4 times more resistive in-core than the HPAM stage at the same rate, an in-situ viscosity asymmetry rather than an elasticity deficit, and a reversal is therefore not claimed. Effluent rheometry in the same source showed no more than a 1% viscosity loss across the core, so glycerol degradation does not explain the offset. The defensible statement is narrower: the published corpus contains no matched-reference support for a secondary-mode elastic advantage, and the frequently cited secondary evidence, as published, is not referenced against an inelastic fluid; the underlying Wreath and Wang thesis data were not available for this screen and are carried as Supportive (Wreath, 1989). The Cottin mode contrast (secondary remaining-oil saturations of 0.09–0.16 versus tertiary 0.23–0.27 at $N_{c,v} \approx 2\times10^{-6}$) is a sweep and displacement-history result, per its own authors. A counter-directional observation also stands: in Bentheimer 11-Y a Newtonian glycerol stage injected after a secondary HPAM flood removed a further 9.6 s.u. once the pressure drop of the preceding HPAM stage was exceeded (Ehrenfried, 2013). Cross-core pairing variability is a residual caveat on the six Ehrenfried pairings, which share three inelastic reference floods, span a threefold permeability spread among the Boise cores, include one rate-mismatched pair, and supply six of the eleven matched secondary comparisons.

3.5 Salinity and relative-permeability channels as quantified scatter sources

Where the elastic sequence also changed brine salinity between stages, the stage-wise desaturation is larger. A comparison is flagged salinity-confounded where the brine changed between the reference stage and the elastic stage of the same contrast; the six Erincik high-salinity stages carry the flag. The Jin sequences also change brine composition: the coreflood-1 waterflood, HPAM stage and glycerin stage each used a different brine, and the source itself attributes part of the second-flood recoveries to the salinity increase. The change there sits outside the contrast rather than inside it, so those comparisons are retained with the history disclosed and the sensitivity reported: removing coreflood 1 moves the paired mean from +0.010 to +0.004. Among tertiary stages classified as high velocity on the velocity-only basis, salinity-changing stages averaged +0.140 saturation units (n = 2) against +0.052 for salinity-constant stages (n = 15, the primary cell pool); across all tertiary stages irrespective of velocity class the corresponding means are +0.123 (n = 6) and +0.056 (n = 32). The difference is descriptive and cannot be assigned independently to salinity: all six flagged stages come from one study, and the stages also differ in sequence, starting saturation and capillary number. In Jin coreflood 1 an inelastic glycerin stage cut S_{or} from 0.238 to 0.07. At the same velocity (1.17 ft/D) and pressure gradient as the preceding elastic stage, at lower capillary number, lower in-situ viscosity (61 against 80 cp) and Deborah number zero, the Newtonian stage removed 1.5 times the oil the elastic stage had removed. Elasticity claims built on stages that simultaneously change salinity are therefore not interpretable as elasticity evidence.

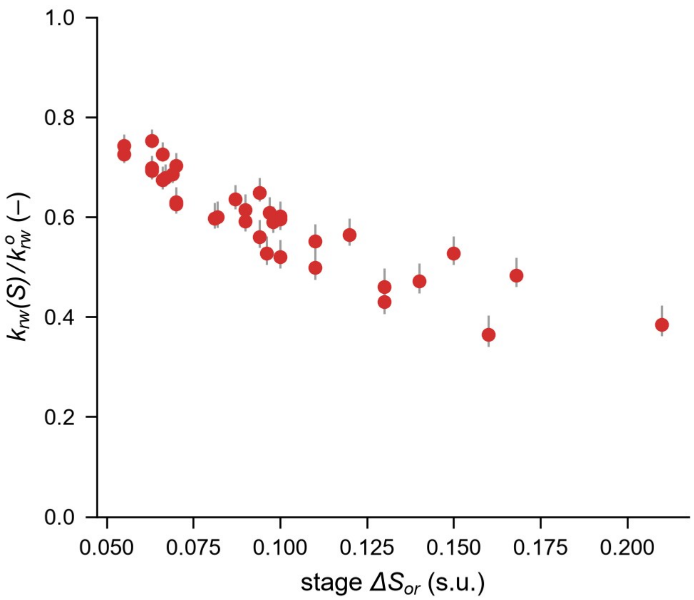

Fig. 5. Endpoint-convention factor $k_{rw}(S)/k_{rw}^{o}$ (Eq. 6) versus stage ΔSor for tertiary stages with ΔSor ≥ 0.05; error bars span n_w = 2.7–3.2.

Because the desaturating stages with the largest ΔS_{or} are precisely those whose endpoint k_{rw} most overstates the in-stage value, convention choice systematically stretches the high end of any compiled curve (Fig. 5): 1.3–2.9× across the admitted tertiary stages, with a single Supportive-tier stage (Koh K4, ΔS_{or} = 0.35) reaching an order of magnitude, shown for range only. Compilations mixing conventions therefore embed a saturation-dependent bias, not merely noise.

3.6 Carbonate injectivity measurements

In-situ resistance factors of a thermally stable ATBS-based polymer (SAV10; powder grade, 4.3–8 MDa per the supplier specifications, at 1,000 ppm; one test with the 12–14-MDa emulsion grade at 800 ppm) and a second commercial polymer (sulfonated, high sulfonation degree, 10–12 MDa per the supplier specification; 1,000 ppm) were measured in six injectivity corefloods on carbonate reservoir cores: permeability 0.0484–0.190 μm² (49–193 md), reported as effective brine permeability at S_{or} for CF-1 and CF-2 (0.0651 and 0.190 μm²; 66 and 193 md), absolute for the three Buhasa cores (0.162, 0.0849 and 0.0484 μm²; 164, 86 and 49 md; at-S_{or} values 0.114 and 0.0286 μm² (116 and 29 md) where measured), and the single-phase core at 0.0799 μm² (81 md); φ = 0.23–0.31, 42,500–243,000 ppm TDS, 50–60 °C; five tests at residual oil saturation (S_{or} = 0.19–0.27) and one single-phase test run in two cycles (Fig. 6); provenance and data basis per Section 2.9. Velocities are interstitial; the basis was confirmed by back-calculation of the reported rate grids against the stated porosities and the reported core diameters (37.6–38.4 mm; agreement within 2%). Resistance factors nearest 0.3048 m/d (1 ft/D) range from 15 to 38 across the at-S_{or} first-run series, and from 7.7 to 72 across all series once the single-phase cycles and post-retention runs are included; with the measured injection-brine viscosity of 1.08 mPa·s (1.08 cp) at 50 °C, the 66-md test corresponds to an apparent in-core viscosity near 41 cp (41 mPa·s) at its 1.31 ft/D (0.400 m/d) grid point (resistance factor 37.97 × 1.08 cp against the same-saturation brine baseline, which is extrapolated at this rate (Section 2.9); equating the product to a viscosity assumes no permeability reduction), which sets the matched-viscosity target for the reference fluid of the designed experiment.

The apparent onset of increasing porous-medium resistance (the velocity at which the resistance factor turns upward) is test-dependent (Table 5): at or below the lowest measured velocity (0.283 m/d; 0.93 ft/D) in one test at S_{or}, a one-sided limit open below; near 0.439 m/d (1.44 ft/D) in a second (bracketed 0.427–1.74 m/d; 1.4–5.7 ft/D); bracketed at 2.01–3.99 m/d (6.6–13.1 ft/D) in the 66-md test (resistance-factor minimum at 2.00 m/d (6.56 ft/D); printed values of 1.83 and 2.13 m/d (6 and 7 ft/D) are roundings of the same grid point); at or below 2.09 m/d (6.9 ft/D) in a fourth, whose two lower-velocity points lack stabilized pressures and are excluded (Section 2.9), so that onset is left-censored rather than bracketed; and history-dependent under repeated slugs, below 0.3048 m/d (1 ft/D) on first injection and near 2.59 m/d (8.5 ft/D) after retention satisfaction in the single-phase test, whose summary table prints < 0.610 m/d (2 ft/D) without resolving cycles and prints 2.74 m/d (9 ft/D) where the recorded grid point is 8.5 ft/D. The second polymer shows the same state dependence within one core: a resistance-factor minimum near 0.446 m/d (1.46 ft/D) in run 2 and no thickening to 26.8 m/d (88 ft/D) in run 3 after further retention.

Table 5. Apparent onset of increasing porous-medium resistance per test (Section 2.9 provenance; onsets in interstitial ft/D, 0.3048 m/d per ft/D). None of the tests separates rate response from progressive retention (ascending-only ladders).

Test	k (md; basis)	Saturation state	Fluid	Apparent onset (ft/D)	Principal caveat
CF-1	66 (effective at S_{or})	S_{or} = 0.25	SAV10 powder, 1,000 ppm	6.6–13.1 (bracket; min 6.56)	brine baseline extrapolated below ≈13 ft/D
CF-2	193 (effective at S_{or})	S_{or} = 0.27	SAV10 emulsion, 800 ppm	≤ 6.9 (left-censored)	two low-rate points excluded; extrapolated baseline
CF-3 (single-phase)	81	single-phase, two cycles	SAV10 powder, 1,000 ppm	< 1 (cycle 1); ≈ 8.5 (cycle 2)	history-dependent; retention not excluded
BU464-6B	164 absolute (116 at S_{or})	S_{or} = 0.20	SAV10 powder, 1,000 ppm	≤ 0.93 (one-sided)	repeat-run RF tracks permeability loss (9, 3; k 116→51→27 md)
BU-86	86 absolute	S_{or} = 0.19	SAV10 powder, 1,000 ppm	1.4–5.7 (bracket; min 1.44)	ascending-only ladder
BU73-4	49 absolute (29 at S_{or})	S_{or} = 0.19	Kemira, 1,000 ppm	≈ 1.46 (run 2); none to 88 (run 3)	run-dependent retention state

Retention, pore plugging, progressive permeability reduction and the extrapolated brine baselines of Section 2.9 are not excluded by these data, and for two tests they are the leading reading: the BU464-6B repeat runs return resistance factors of 9 and 3 near 1 ft/D as the brine permeability at S_{or} falls from 116 to 51 to 27 md, a decline reproduced within the stated precision by the permeability ratio alone (18.75 × 51/116 = 8.2), and the single-phase test's cycle-2 curve sits a factor of 7–9 above cycle 1 below onset. No bulk viscosity in the make-up brine and no residual resistance factor were recorded for these tests, so the resistance factor cannot be decomposed into a viscosity part and a permeability-reduction part; published decompositions in comparable carbonates attribute a factor of 2.2–4.8 to permeability reduction (Masalmeh et al., 2019; Alfazazi et al., 2021). Every test used an ascending-only rate ladder, so progressive retention and rate response are not separable in any of the six; the rise is reported as an apparent increase in porous-medium resistance rather than as a demonstrated elastic transition.

The order-of-magnitude spread across nominally similar tests indicates that the onset is a system property (polymer, brine, temperature, retention history and core) and must be measured for the system of interest rather than imported. Independent carbonate observations carry the same message with a direction that is itself contested: with a high-ATBS-content polyacrylamide in a 412-md (0.407 μm²) reservoir-carbonate core (107 md at residual oil), shear thickening weakened once residual oil was established, in a comparison made against a different, water-saturated core that the source itself flags as anomalous (Masalmeh et al., 2019); with an ATBS-acrylamide copolymer in Indiana limestone, the source's own summary reads the thickening onset as reduced in the presence of crude oil while a later reading of the same figures reports it increased (Alfazazi et al., 2021; Seright et al., 2023). The two sources also plot velocity on different bases (Darcy and interstitial respectively), so magnitudes are not directly comparable across the three data sets without conversion.

The spread is consistent with a chemistry effect dominating the pore-geometry scaling of Eq. 3: scaling a nominal 1 ft/D (0.3048 m/d) onset for an 18-MDa HPAM in a 2,000-md, φ = 0.22 sandstone by the geometric term alone places the onset near 0.18–0.37 ft/D (0.055–0.113 m/d) in these cores, and the k_{rw} and oil-saturation terms of the published at-residual shift factor (Seright et al., 2023) lower it further, whereas the measured onsets for the 4.3–8-MDa ATBS-based polymer lie a factor of 5–30 higher, the direction expected from the shorter extensional relaxation time of the lower-molecular-weight backbone; relaxation times were not measured for either fluid. The second polymer, at 10–12 MDa, showed no thickening to 88 ft/D in its final run, so the behaviour is not generalized to a polymer class and molecular weight alone does not order the onsets.

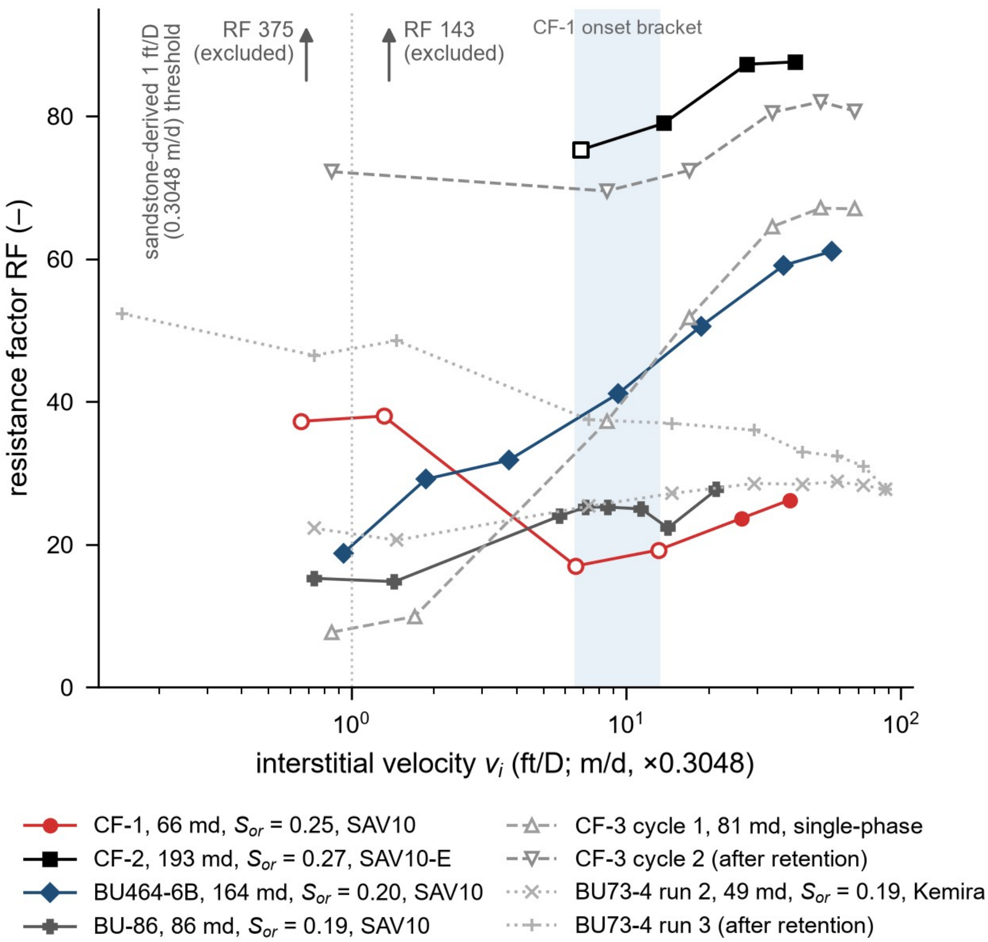

Fig. 6. In-situ resistance factor versus interstitial velocity for polymer injectivity tests in carbonate reservoir cores (SAV10 ATBS-based powder at 1,000 ppm and emulsion at 800 ppm; second commercial sulfonated polymer, 10–12 MDa, at 1,000 ppm; permeability 0.0484–0.190 μm² (49–193 md), effective at S_{or} for CF-1/CF-2 and absolute for the Buhasa cores; five tests at S_{or} = 0.19–0.27, one single-phase in two cycles; 50–60 °C; 42,500–243,000 ppm TDS). Shaded band: onset bracket of the 0.0651 μm² (66-md) test at S_{or} (2.01–3.99 m/d; 6.6–13.1 ft/D). Dotted line: sandstone-derived 1 ft/D (0.3048 m/d) threshold. Point-by-point basis tags (reported, digitized, derived) are carried in the supplementary dataset; unstable low-rate points are excluded per Section 2.9.

4. Discussion

4.1 What the screened record can and cannot say

The affirmative and skeptical positions are each supported under restricted conditions. Matched-reference elastic increments of at least 0.10 saturation units occurred in salinity-unconfounded tertiary comparisons at interstitial velocities of 1 ft/D (0.3048 m/d) and above. That is the operating window of the affirmative studies, with five of the eight at exactly the boundary, among them the Clarke comparison at exactly 0.10 s.u. The null results lie at low flow intensity (the accessibility caveat of Seright and Wang (2023)), low elasticity (Sandengen et al., 2017), stages following an earlier viscous flood, or heavy oil (the 300-cp (300 mPa·s) Vermolen secondary flood), although positive increments at 120 cp (120 mPa·s) (Qi) show that oil viscosity alone does not sort the record. But conditional structure at the stage level is not proof at the study level: with seven studies, four of one laboratory lineage (a fifth of the same lineage is Supportive), the study-resampling bootstrap (approximate at six clusters) cannot exclude a zero velocity effect ([−0.063, +0.023] on the stage-level difference), the leave-one-out analysis reverses the sign of the paired mean on removal of Qi alone, and the Grade-A-referenced subset holds a single comparison above the boundary. The screened record therefore supports a narrow statement and cannot support the broader statement either way. Increments above a matched viscous reference have been reported only at interstitial velocities of 1 ft/D and above in tertiary mode, while that same regime also contains contrasts of 0.013 saturation units and below, including three at or under 0.002. At four paired studies with the observed spread, only a velocity effect larger than approximately 0.06 saturation units in magnitude would have been resolvable; the record therefore measures the literature's resolving power, not the effect. A continuous treatment makes the same point from the other side: regressing ΔS_{or} on the base-10 logarithm of v_i across the 32 unconfounded tertiary contrasts returns +0.026 saturation units per order of magnitude of velocity (study-clustered standard error 0.005; study-clustered bootstrap p = 0.078 at six clusters; $R^2 = 0.05$), sign-stable to removal of any study (+0.022 to +0.039) where the two-cell contrast reverses sign. The slope is not separable from zero at six clusters, and velocity remains confounded with study identity and reference grade (Section 3.3), so it is reported as a specification sensitivity, not a finding. Sections 4.3 and 4.4 therefore specify better-designed primary data rather than another re-analysis.

4.2 Field-velocity application of the measured onset range

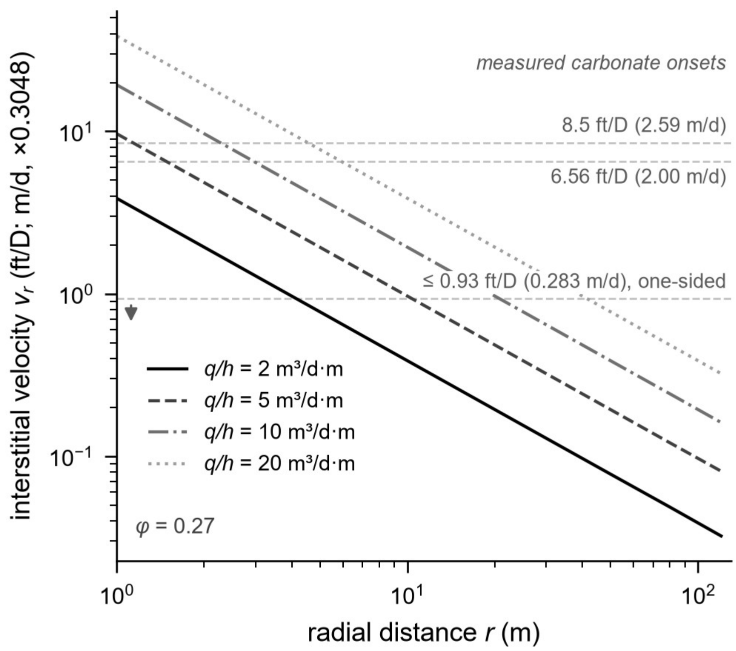

Fig. 7. Radial interstitial-velocity decay around an unfractured vertical injector for representative q/h at φ = 0.27, against the measured carbonate onset velocities of 0.3048, 2.13 and 2.74 m/d (1, 7 and 9 ft/D) (Eq. 7; Section 3.6). Radii scale as 1/φ over the measured porosity range 0.23–0.31.

Table 6. Radius r* inside which the interstitial velocity exceeds the measured carbonate onsets of Section 3.6 (Eq. 7, φ = 0.27).

q*/*h **(m³/d per m)**	***r* at 1 ft/D (0.3048 m/d) (m)***	***r* at 7 ft/D (2.13 m/d) (m)***	***r* at 9 ft/D (2.74 m/d) (m)***
2	3.9	0.55	0.43
5	9.7	1.4	1.1
10	19.3	2.8	2.1
20	38.7	5.5	4.3

At a representative q/h of 10 m³/d per metre and φ = 0.27, the measured carbonate onsets of Section 3.6 are exceeded only close to an unfractured vertical injector: within approximately 19–24 m for the at-or-below-1-ft/D onset (0.283–0.3048 m/d; the lowest onset is a one-sided limit, so larger radii are not excluded) and within approximately 2–3 m for the 2.13–2.74 m/d (7–9 ft/D) onsets (Fig. 7; Table 6); radii scale as 1/φ across the measured 0.23–0.31 porosity range. The field-velocity argument was raised in Seright and Wang (2023) and developed by Azad and Seright (2025), whose deep-pattern analysis (0.01–0.2 ft/D (0.00305–0.0610 m/d) typical, under one percent of pattern volume above onset) and exceptions (close spacing, ≈1.7 ft/D (0.518 m/d) at Pelican-Lake-type geometry; Daqing throughput of 0.14–0.20 PV/yr at 150–250-m spacing (Wang et al., 2008b)) are reproduced here as an application of the measured onsets rather than as a new result. The screening statement follows: viscoelastic S_{or} credit, where claimed at all, belongs only to the reservoir volume that the radial bound or a fracture/thin-bed equivalent places above onset. Resistance factors of the magnitude measured in Section 3.6 (15–75) are themselves difficult to sustain in an unfractured vertical well; comparable factors have been argued to force open fractures regardless of the assumed rheology (Seright et al., 2023). The unfractured single-layer geometry is therefore a screening idealization in this respect as well. The bound delimits where elastic flow resistance is possible; it does not locate desaturation.

Screening summary for practice. (i) Where a forecast books incremental S_{or} from viscoelasticity, the credited volume must lie inside the onset radius (Table 6: approximately 19 m at q/h = 10 m³/d per metre for a 1 ft/D (0.3048 m/d) onset; 2–3 m for the 6.6–8.5 ft/D onsets) or be placed above onset by fractures or thin high-flux layers; otherwise the credit has no laboratory-supported route. (ii) The onset does not transfer between systems: across six related carbonate cores it moved from at or below 0.93 ft/D (0.283 m/d) to 6.6–13.1 ft/D (2.01–3.99 m/d) and was history-dependent (Section 3.6), so it is measured for the actual polymer–brine–rock system, not imported from sandstone. (iii) Laboratory evidence offered for the credit satisfies the checklist of Section 4.3, with the matched-viscosity target derived as in Section 3.6.

4.3 A proposed minimum reporting checklist for elastic-versus-reference corefloods

The screen that reduced 39 published studies to seven usable studies is itself the clearest statement of what the literature lacks. It is restated here as a prospective checklist; a future coreflood that satisfies it enters this framework directly; one that does not cannot be placed on a common basis with the admitted set.

R1. A matched inelastic reference in the same study, with the grade declared: Grade A (xanthan, scleroglucan, or a low-elasticity polymer matched on in-situ apparent viscosity from pressure drop) preferred over Grade B (glycerol), whose temperature and dilution sensitivity and Newtonian in-core behaviour make bulk matching unequal in-situ matching (motivating defect: bulk-matched glycerol referencing, Sections 2.8 and 3.3).

R2. Matched capillary number between elastic stage and reference: matched pressure gradient by design, or reported ΔN_c within 0.5 log10 units (motivating defect: unmatched capillary number in the flagged comparisons of Appendix B, Table B.1 D2).

R3. Constant brine salinity across all stages of a sequence; salinity changes reported as separate, labelled stages (motivating defect: the low-to-high-salinity sequences of Section 3.5).

R4. Velocity reported with its basis (interstitial versus Darcy), together with the pressure gradient per stage, so both capillary-number conventions are computable (motivating defect: mixed and undeclared velocity bases across the corpus, Section 2.3).

R5. Endpoint saturations per stage by at least two independent methods, with stage-wise injected pore volumes, so throughput-limited nulls are distinguishable from true nulls (motivating defect: recovery-basis reporting, the largest single cause of Supportive-tier demotion in Appendix B).

R6. End-effect evidence: a rate ladder or Rapoport–Leas number per stage, or in-situ saturation profiles (motivating defect: unmitigated capillary end effects in the early corefloods of Section 1.1).

R7. Saturation-dependent water relative permeability (or at minimum the Corey exponent), so flux-based capillary numbers are not silently endpoint-biased (motivating defect: the endpoint-convention bias quantified in Section 2.5).

R8. For secondary-mode designs, sequential single-core referencing with an order-reversal control in preference to cross-core twins, which inherit core variability (motivating defect: the cross-core twins of Section 3.4).

4.4 The carbonate gap and the designed experiment

No carbonate study satisfying the admission criteria was identified in the screened corpus at the 3 August 2026 search cutoff; the admitted set is entirely sandstone and sandpack, and the closest near-miss (Dhahir et al., 2026) fails on in-situ reference matching and constant-salinity grounds (Appendix B). The absence is most consequential where polymer programmes are advancing into high-temperature, high-salinity carbonates (Fabbri et al., 2021). Two classes of existing carbonate data short of the full experiment are nevertheless useful within this framework. First, polymer injectivity data measure in-situ flow resistance versus velocity at and away from residual oil, a design consolidated in sandstone by Seright et al. (2023), and in carbonate cores therefore bound the apparent onset of increasing porous-medium resistance in carbonate pore structure; the measurements are reported in Section 3.6. Second, surfactant and surfactant–polymer corefloods at residual conditions in carbonates locate where carbonate S_{or} begins to move under interfacial-tension reduction; they are not elasticity evidence, because the interfacial-tension reduction dominates and no inelastic reference exists, but they bound what any elastic mechanism would have to exceed; those anchors are not compiled here.

Applied through Eq. 7 at q/h = 10 m³/d per metre with per-test porosities, the measured range places the regime of measured resistance onset within approximately 2.4 m (onset 8.5 ft/D (2.59 m/d), φ = 0.256) to 24 m (onset at or below 0.93 ft/D (0.283 m/d), φ = 0.23) of an unfractured vertical injector; the bracket uses per-test onset-porosity pairs, and at fixed φ = 0.27 the onset range alone spans approximately 2.3–19 m. Because the lowest onset is a one-sided limit, radii above 24 m are not excluded. Elastic flow resistance is a necessary condition for any viscoelastic desaturation mechanism, not a demonstration of it; whether desaturation accompanies the measured onset is the question the designed experiment answers. The mechanism hypothesised to underlie the onset and the resulting screening geometry are sketched in Fig. 8.

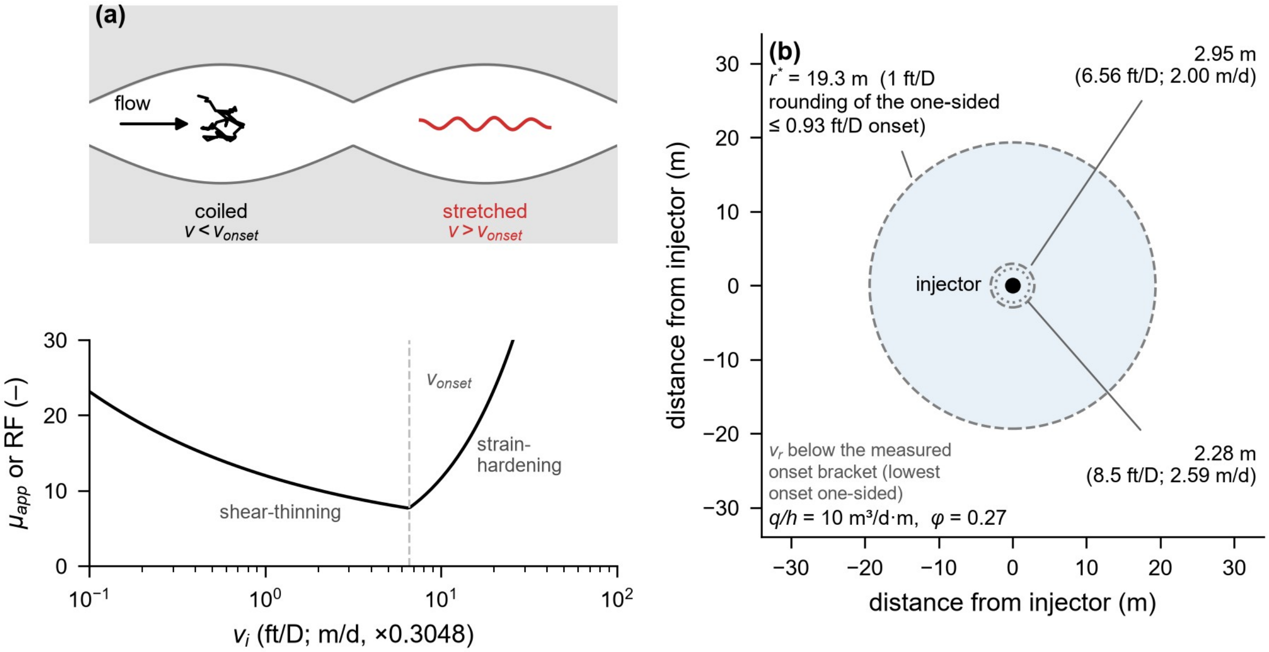

Fig. 8. Hypothesised mechanism and screening geometry (schematic). (a) Coil-stretch transition in a converging-diverging pore, the mechanism under test and not demonstrated by these data: below the onset velocity the macromolecule transits coiled and the apparent viscosity shear-thins; above it the elongation rate is sufficient for chain extension and flow resistance rises. (b) Plan view of the radial screen (Eq. 7) at q/h = 10 m³/d per metre and generic φ = 0.27 (per-test porosities differ; Section 4.2): the measured onset brackets place the resistance-onset regime within approximately 2.3–19.3 m of an unfractured vertical injector; the lowest onset is one-sided, so the outer radius is not excluded upward.

The matched-reference experiment is then fully specified by the checklist of Section 4.3. Design: a single low-permeability carbonate core at restored wettability, waterflooded to true residual with a rate ladder and Rapoport–Leas documentation (R6); a tertiary Grade-A inelastic reference, at HTHS conditions a low-elasticity sulfonated polymer matched on in-situ apparent viscosity rather than glycerol (R1), injected at matched pressure gradient to stabilization with stage pore volumes logged (R2, R5); then the viscoelastic ATBS/HPAM stage at the same in-situ apparent viscosity and gradient below the onset, and above the onset at held velocity with the resulting gradient and ΔN_c reported, since matched viscosity, matched gradient and matched velocity cannot hold simultaneously once the elastic fluid thickens; the elastic stage stepped through a velocity ladder bracketing the measured onset range of Fig. 6 (0.283–2.59 m/d interstitial; 0.93–8.5 ft/D, open below), ascending and then descending so that progressive retention is separable from rate response, a control absent from the Section 3.6 tests (R2, R4); brine salinity held constant throughout (R3); endpoint saturations by material balance plus tracer or X-ray (R5); and saturation-dependent k_{rw} taken from the reference stage (R7). Scleroglucan requires demonstrated stability in the target brine before selection, and the matched-viscosity target may need to sit below the 41 cp (41 mPa·s) of Section 3.6 if no sufficiently inelastic fluid reaches it at 243,000 ppm and 50–60 °C. A second core runs the order-reversal control (elastic stage first, inelastic chase), the simplest discriminating control in the corpus; the Daqing study (Wang et al., 2000) and Bentheimer 11-Y (Ehrenfried, 2013) disagree on what it shows. Outcomes are pre-registered against the competing hypotheses: an elastic increment above the reference at matched N_c that grows through the onset supports field-conditional viscoelastic desaturation in carbonates; identical endpoints support the artifact reading; an inelastic chase recovering further oil after the elastic stage indicates the in-situ viscosity channel. The gradient requirement is bounded: at 41 cp and 29–49 md, the 0.93–8.5 ft/D ladder implies approximately 35–550 psi/ft (0.79–12.4 MPa/m). That is executable in a standard core holder but far above field gradients, so outcomes are read as screening physics, not field response. The Grade-A reference stage itself operates at $N_{c,v}$ of roughly 7×10^{-6} to 6×10^{-5} across the ladder and can desaturate the core by ordinary capillary means; the order-reversal control exists to bound that channel. A single core pair resolves the mechanism only for the system tested and does not establish a population effect; the pre-registered outcomes are stated so the result enters the framework of Section 4.3 as one study, and the checklist is written so further studies accumulate on a common basis. One such pair of floods would provide admissible carbonate evidence on either side of the question, which the screened corpus does not currently supply.

5. Conclusions

1. Of thirty-nine inventoried published studies, seven studies satisfy the matched-inelastic-reference screen, yielding 49 elastic-versus-reference contrasts; Cottin et al. are retained as Supportive mode-contrast evidence. The screen, the per-value provenance, the exclusion log, and the statistical guards against non-independence are the methodological contribution; the extensional capillary number used for replotting is prior art (Azad and Trivedi, 2021, 2023) whose implementation reproduces the published pore-scale viscosities to better than 0.4% on the source's own velocity convention.

2. The corpus does not resolve an independent velocity effect attributable to polymer viscoelasticity; this is the central finding. The paired within-study difference across the four studies carrying both velocity regimes is +0.010 saturation units with a paired interval at three degrees of freedom of [−0.046, +0.066]; only an effect larger than approximately 0.06 saturation units in magnitude would have been resolvable at this corpus size, so the record measures the literature's resolving power rather than the effect. At the stage level the velocity-only tertiary cells do not separate (+0.052 against +0.059, n = 15 and 17); an ordering appears only under boundary reassignment (+0.068 against +0.036) or under the superseded classifier; and every salinity-unconfounded tertiary increment of at least 0.10 saturation units lies at 1 ft/D (0.3048 m/d) or above. The corpus likewise contains no matched-reference support for a secondary-mode elastic advantage: the matched secondary comparisons average approximately zero against Grade-A references at the stage level, reverse sign at the study level, and run negative against glycerol, a pattern consistent with the measured in-core viscosity offset of the glycerol references rather than with an elasticity deficit.

3. Two quantified channels inflate apparent scatter in compiled desaturation curves: stage-wise salinity change (exceeding the unconfounded elasticity channel) and the endpoint-k_{rw} convention (a 1.3–2.9-fold capillary-number bias across the admitted stages, saturation-dependent and therefore systematic rather than random).

4. New in-situ measurements in six carbonate reservoir cores place the apparent onset of increasing porous-medium resistance for the polymers tested between at or below 0.93 ft/D (0.283 m/d) and 6.6–13.1 ft/D (2.01–3.99 m/d), history-dependent and absent to 88 ft/D (26.8 m/d) in one run; retention, pore plugging and progressive permeability reduction are not excluded by ascending-rate data, and the onsets are system properties to be measured, not imported. Applied through the radial bound at q/h = 10 m³/d per metre with per-test porosities, the measured range confines the corresponding flow regime to approximately 2.4–24 m around an unfractured vertical injector, open above because the lowest onset is one-sided; elastic flow resistance is a necessary condition for viscoelastic desaturation, not a demonstration of it. The constructive output is a proposed minimum reporting checklist (Section 4.3) and a fully specified matched-reference carbonate experiment (Section 4.4) that uses the measured onset range in place of the sandstone threshold; one compliant flood pair would add evidence the existing record cannot supply under any re-analysis.

Nomenclature

Symbols

C	shear-rate coefficient in Eq. 3, dimensionless
h	completed interval thickness, m
k	permeability, md (9.86923×10⁻⁴ μm² per md; m² in equations)
k_{rw}	water relative permeability, dimensionless
k_{rw}^{o}	endpoint water relative permeability, dimensionless
n	shear-thinning exponent, dimensionless
n_2	strain-hardening index (source usage: shear-thickening exponent), dimensionless
n_w	Corey water exponent, dimensionless
$N_{c,v}$	velocity-based capillary number, dimensionless
$N_{c,\Delta p}$	pressure-gradient-based capillary number, dimensionless
N_{ce}	extensional capillary number, dimensionless
ΔN_c	$\log_{10}$ offset between elastic-stage and reference capillary number, dimensionless
q	injection rate, m³/d
r	radial distance, m
r^*	onset radius, m
S	saturation, fraction
S_{or}	residual oil saturation, fraction
S_{wi}	initial water saturation, fraction
S_{wr}	residual water saturation, fraction
ΔS_{or}	stage change in residual oil saturation, saturation units
u	superficial (Darcy) flux, ft/D (0.3048 m/d per ft/D; m/s in equations)
v_{onset}	interstitial onset velocity in Eq. 7, ft/D (0.3048 m/d per ft/D)
u_r	radial Darcy velocity, ft/D (0.3048 m/d per ft/D)
v_r	radial interstitial velocity (= u_r/φ), ft/D (0.3048 m/d per ft/D)
v_i	interstitial velocity, ft/D (0.3048 m/d per ft/D; m/s in equations)

Greek

α	model constant in Eq. 4, dimensionless
β	model constant in Eq. 4, dimensionless

$\dot{\gamma}$	in-situ shear rate, 1/s
λ	time constant in Eq. 4, s
μ	viscosity, cp (≡ mPa·s; Pa·s in equations)
μ_{app}	apparent viscosity, cp (≡ mPa·s; Pa·s in equations)
μ_{p0}	zero-shear polymer-solution viscosity in Eq. 4, cp (≡ mPa·s)
μ_{∞}	infinite-shear (solvent-limit) viscosity in Eq. 4, cp (≡ mPa·s)
μ_{max}	shear-thickening plateau viscosity in Eq. 4, cp (≡ mPa·s)
σ	oil–water interfacial tension, mN/m
τ_{ext}	extensional relaxation time, s
φ	porosity, fraction
∇p	pressure gradient, psi/ft (22.6206 kPa/m per psi/ft)

Abbreviations

ATBS	acrylamide tertiary-butyl sulfonate
CDC	capillary desaturation curve
EDC	elastic desaturation curve (Deborah-based; Qi et al., 2018)
HPAM	partially hydrolyzed polyacrylamide
HS	high salinity
HTHS	high temperature, high salinity
LS	low salinity
RF	resistance factor: stabilized polymer-to-brine pressure-drop ratio at equal rate, dimensionless
IFT	interfacial tension
s.u.	saturation units

Declarations

Author contributions (CRediT): Imad A. Adel: Conceptualization, Methodology, Data curation, Formal analysis, Investigation, Software, Visualization, Writing – original draft, Writing – review & editing. **Alvaro Hernandez:** Conceptualization, Investigation, Formal analysis, Writing – review & editing. **Emad W. Al-Shalabi:** Investigation, Project administration, Supervision, Writing – review & editing.

Data availability: Data supporting the findings of this study are available from the corresponding author upon reasonable request. The extracted literature values with per-value provenance, the statistical outputs, and the source data for every figure are provided as a supplementary dataset (Tables S4 and S5), from which all figures regenerate.

Declaration of competing interest: The authors declare that they have no known competing financial interests or personal relationships that could have appeared to influence the work reported in this paper.

Acknowledgements: This research was funded by Khalifa University of Science and Technology through the ADNOC Grant Call under Project ID: KU-EXT-ADNOC-2022-8434000317. This research was supported by the Research and Innovation Center on CO_2 and Hydrogen (RICH), Khalifa University of Science and Technology.

References

Abrams, A., 1975. The influence of fluid viscosity, interfacial tension, and flow velocity on residual oil saturation left by waterflood. SPE Journal 15 (5), 437-447. SPE-5050-PA. https://doi.org/10.2118/5050-PA

Alfazazi, U., Thomas, N.C., Al-Shalabi, E.W., AlAmeri, W., 2021. Investigation of oil presence and wettability restoration effects on sulfonated polymer retention in carbonates under harsh conditions. In: Abu Dhabi International Petroleum Exhibition and Conference, Abu Dhabi, UAE. SPE-207892-MS. https://doi.org/10.2118/207892-MS

Azad, M.S., Seright, R.S., 2025. Are field polymer enhanced oil recovery projects reaping the benefits of residual oil saturation reduction due to polymer viscoelasticity? SPE Journal 30 (6), 3792-3809. SPE-223155-PA. https://doi.org/10.2118/223155-PA

Azad, M.S., Trivedi, J.J., 2019. Quantification of the viscoelastic effects during polymer flooding: a critical review. SPE Journal 24 (6), 2731-2757. SPE-195687-PA. https://doi.org/10.2118/195687-PA

Azad, M.S., Trivedi, J.J., 2021. Quantification of Sor reduction during polymer flooding using extensional capillary number. SPE Journal 26 (3), 1469-1498. SPE-204212-PA. https://doi.org/10.2118/204212-PA

Azad, M.S., Trivedi, J.J., 2023. Quantification of polymer viscoelastic effects on Sor reduction using modified capillary number. U.S. Patent 11,761,331, issued 19 September 2023.

Barri, A., Azad, M.S., Al-Shehri, D., Ayirala, S.C., Patil, S., Al-Hamad, J., Abdullah, E., Al Abdrabalnabi, R., 2023. Is there a viscoelastic effect of low-MW HPAM polymers on residual oil mobilization in low-permeability rocks at a Darcy velocity of 0.2 ft/day? Energy & Fuels 37, 10188-10199. https://doi.org/10.1021/acs.energyfuels.3c00955

Chatzis, I., Morrow, N.R., 1984. Correlation of capillary number relationships for sandstone. SPE Journal 24 (5), 555-562. SPE-10114-PA. https://doi.org/10.2118/10114-PA

Clarke, A., Howe, A.M., Mitchell, J., Staniland, J., Hawkes, L.A., 2016. How viscoelastic-polymer flooding enhances displacement efficiency. SPE Journal 21 (3), 675-687. SPE-174654-PA. https://doi.org/10.2118/174654-PA

Cottin, C., Bourgeois, M., Bursaux, R., Jimenez, J., Lassalle, S., 2014. Secondary and tertiary polymer flooding on highly permeable reservoir cores: experimental results. In: SPE EOR Conference at Oil and Gas West Asia, Muscat, Oman. SPE-169692-MS. https://doi.org/10.2118/169692-MS

Dafaalla, M., Azad, M.S., Ayirala, S., Alotaibi, M., Fahmi, M., Saleh, S., Al Shehri, D., Mahmoud, M., 2025. Potential of polymer's viscosity and viscoelasticity for accessible oil recovery during low salinity polymer flooding in heterogeneous carbonates. Fuel 379, 133008. https://doi.org/10.1016/j.fuel.2024.133008

Dhahir, D., Azad, M.S., Alotaibi, M., 2026. Examining the desaturation potential of low and high-salinity viscoelastic polymer solutions at high salinity and high temperature carbonate reservoir conditions. In: SPE Improved Oil Recovery Conference held in Tulsa, Oklahoma, USA 21–23 April 2026. SPE-231553-MS. https://doi.org/10.2118/231553-MS

Du, Y., Xu, K., Mejia, L., Balhoff, M., 2021. A coreflood-on-a-chip study of viscoelasticity's effect on reducing residual saturation in porous media. Water Resources Research 57 (8), e2021WR029688. https://doi.org/10.1029/2021WR029688

Ehrenfried, D.H., 2013. Impact of viscoelastic polymer flooding on residual oil saturation in sandstones. MS Thesis, The University of Texas at Austin, Austin, Texas, USA.

Erincik, M.Z., Qi, P., Balhoff, M.T., Pope, G.A., 2017. New method to reduce residual oil saturation by polymer flooding. In: SPE Annual Technical Conference and Exhibition, San Antonio, Texas, USA. SPE-187230-MS. https://doi.org/10.2118/187230-MS

Erincik, M.Z., Qi, P., Balhoff, M.T., Pope, G.A., 2018. New method to reduce residual oil saturation by polymer flooding. SPE Journal 23 (5), 1944-1956. SPE-187230-PA. https://doi.org/10.2118/187230-PA

Laudon, S., Balhoff, M., Mohanty, K., 2024. The effect of polyethylene oxide polymer injection on residual oil saturation of Indiana limestone. In: SPE Improved Oil Recovery Conference, Tulsa, Oklahoma, USA. SPE-218150-MS. https://doi.org/10.2118/218150-MS

Laudon, S., Balhoff, M., Mohanty, K., 2026. The effect of polyethylene oxide polymer injection on residual oil saturation of Indiana limestone. Geoenergy Science and Engineering 264, 214549. https://doi.org/10.1016/j.geoen.2026.214549

Fabbri, C., Al Saadi, H.A., Wang, K., Maire, F., Romero, C., Cordelier, P., Prinet, C., Jouenne, S., Garnier, O., Xu, S., Leon, J.M., Baslaib, M., Masalmeh, S., 2021. Polymer injection to unlock bypassed oil in a giant carbonate reservoir: bridging the gap between laboratory and large scale polymer project. In: Abu Dhabi International Petroleum Exhibition and Conference, Abu Dhabi, UAE. SPE-208121-MS. https://doi.org/10.2118/208121-MS

Guo, H., Song, K., Hilfer, R., 2022. A brief review of capillary number and its use in capillary desaturation curves. Transport in Porous Media 144, 3-31. https://doi.org/10.1007/s11242-021-01743-7

Huh, C., Pope, G.A., 2008. Residual oil saturation from polymer floods: laboratory measurements and theoretical interpretation. In: SPE Symposium on Improved Oil Recovery, Tulsa, Oklahoma, USA. SPE-113417-MS. https://doi.org/10.2118/113417-MS

Humphry, K.J., Suijkerbuijk, B.M.J.M., van der Linde, H.A., Pieterse, S.G.J., Masalmeh, S.K., 2014. Impact of wettability on residual oil saturation and capillary desaturation curves. Petrophysics 55 (4), 313–318.

Irfan, M., Stephen, K.D., Lenn, C.P., 2021. An experimental study to understand polymer viscoelasticity effect on residual oil saturation at elevated temperature. Upstream Oil and Gas Technology 6, 100026. https://doi.org/10.1016/j.upstre.2020.100026

Jain, H., Azad, M.S., Ayirala, S., Mahmoud, M., Al Shehri, D., Fahmi, M., 2026. Viscoelasticity vs. viscosity: what dominates the Sor reduction at shear thinning flux in low permeable limestone cores at low salinity polymer flood conditions? Results in Engineering 30, 110897. https://doi.org/10.1016/j.rineng.2026.110897

Jameel, M.F., Azad, M.S., Adebayo, A.R., Ayirala, S., Al Shehri, D., Mahmoud, M., 2026. IFT vs. viscoelasticity: what is the most potent microscopic light oil recovery mechanism in water-wet high-permeable formations? In: SPE Improved Oil Recovery Conference held in Tulsa, Oklahoma, USA 21–23 April 2026. SPE-231475-MS. https://doi.org/10.2118/231475-MS

Jiang, H.F., Wu, W.X., Wang, D.M., Zeng, Y.M., Zhao, S.G., Nie, J., 2008. The effect of elasticity on displacement efficiency in the lab and results of high concentration polymer flooding in the field. In: SPE Annual Technical Conference and Exhibition, Denver, Colorado, USA. SPE-115315-MS. https://doi.org/10.2118/115315-MS

Jin, J., Qi, P., Mohanty, K., Balhoff, M.T., 2020. Experimental investigation of the effect of polymer viscoelasticity on residual saturation of low viscosity oils. In: SPE Improved Oil Recovery Conference, Tulsa, Oklahoma, USA. SPE-200414-MS. https://doi.org/10.2118/200414-MS

Koh, H., 2015. Experimental investigation of the effect of polymers on residual oil saturation. PhD Dissertation, The University of Texas at Austin, Austin, Texas, USA.

Koh, H., Lee, V.B., Pope, G.A., 2018. Experimental investigation of the effect of polymers on residual oil saturation. SPE Journal 23 (1), 1-17. SPE-179683-PA. https://doi.org/10.2118/179683-PA

Masalmeh, S., AlSumaiti, A., Gaillard, N., Daguerre, F., Skauge, T., Skauge, A., 2019. Extending polymer flooding towards high-temperature and high-salinity carbonate reservoirs. In: Abu Dhabi International Petroleum Exhibition and Conference, Abu Dhabi, UAE. SPE-197647-MS. https://doi.org/10.2118/197647-MS

Qi, P., Ehrenfried, D.H., Koh, H., Balhoff, M.T., 2017. Reduction of residual oil saturation in sandstone cores by use of viscoelastic polymers. SPE Journal 22 (2), 447-458. SPE-179689-PA. https://doi.org/10.2118/179689-PA

Qi, P., Lashgari, H., Luo, H., Delshad, M., Pope, G.A., Balhoff, M.T., 2018. Simulation of viscoelastic polymer flooding - from the lab to the field. In: SPE Annual Technical Conference and Exhibition, Dallas, Texas, USA. SPE-191498-MS. https://doi.org/10.2118/191498-MS

Sandengen, K., Melhuus, K., Kristoffersen, A., 2017. Polymer ‘viscoelastic effect’; does it reduce residual oil saturation. Journal of Petroleum Science and Engineering 153, 355-363. https://doi.org/10.1016/j.petrol.2017.03.029

Seright, R.S., Azad, M.S., Abdullah, M.B., Delshad, M., 2023. Effect of residual oil saturation and salinity on HPAM rheology in porous media. In: SPE Annual Technical Conference and Exhibition, San Antonio, Texas, USA. SPE-215060-MS. https://doi.org/10.2118/215060-MS

Seright, R.S., Wang, D., 2023. Polymer flooding: current status and future directions. Petroleum Science 20, 910-921. https://doi.org/10.1016/j.petsci.2023.02.002

Vermolen, E.C.M., van Haasterecht, M.J.T., Masalmeh, S.K., 2014. A systematic study of the polymer visco-elastic effect on residual oil saturation by core flooding. In: SPE EOR Conference at Oil and Gas West Asia, Muscat, Oman. SPE-169681-MS. https://doi.org/10.2118/169681-MS

Wang, D., Cheng, J., Yang, Q., Gong, W., Li, Q., Chen, F., 2000. Viscous-elastic polymer can increase microscale displacement efficiency in cores. In: SPE Annual Technical Conference and Exhibition, Dallas, Texas, USA. SPE-63227-MS. https://doi.org/10.2118/63227-MS

Wang, D., Cheng, J., Xia, H., Li, Q., Shi, J., 2001a. Viscous-elastic fluids can mobilize oil remaining after water-flood by force parallel to the oil-water interface. In: SPE Asia Pacific Improved Oil Recovery Conference, Kuala Lumpur, Malaysia. SPE-72123-MS. https://doi.org/10.2118/72123-MS

Wang, D., Xia, H., Liu, Z., Yang, Q., 2001b. Study of the mechanism of polymer solution with visco-elastic behavior increasing microscopic oil displacement efficiency and the forming of steady oil thread flow channels. In: SPE Asia Pacific Oil and Gas Conference and Exhibition. SPE-68723-MS. https://doi.org/10.2118/68723-MS

Wang, D., Han, P., Shao, Z., Chen, J., Seright, R.S., 2008a. Sweep-improvement options for the Daqing oil field. SPE Reservoir Evaluation & Engineering 11 (1), 18–26. SPE-99441-PA. https://doi.org/10.2118/99441-PA

Wang, D., Seright, R.S., Shao, Z., Wang, J., 2008b. Key aspects of project design for polymer flooding at the Daqing oilfield. SPE Reservoir Evaluation & Engineering 11 (6), 1117-1124. SPE-109682-PA. https://doi.org/10.2118/109682-PA

Wreath, D., 1989. A study of polymer flooding and residual oil saturation. MS Thesis, The University of Texas at Austin, Austin, Texas, USA (Antolini/Szabo dataset; cited in Huh and Pope, 2008; full text not obtained).

Zeynalli, M., Mushtaq, M., Al-Shalabi, E.W., Alfazazi, U., Hassan, A.M., AlAmeri, W., 2023. A comprehensive review of viscoelastic polymer flooding in sandstone and carbonate rocks. Scientific Reports 13, 17679. https://doi.org/10.1038/s41598-023-44896-9

Appendix A. Admitted-study summary

One row per admitted study. The full 112-row per-stage dataset with basis tags, fluid descriptors and per-value provenance is supplementary Table S4 (Supportive rows there are display-only and enter no statistic); the 49 contrasts with construction basis, in-core-reference status and injection order are supplementary Table S5. Values are in the first-listed unit of each column header. The legacy intensity classifier is retained only in the supplementary tables, labelled as such; the primary analysis classifies on interstitial velocity alone, v_i > 1 ft/D (0.3048 m/d), strict.

Study	Lineage	k (md)	μo (cp)	Stages / contrasts	Ref. grade(s)
QI17	UT Austin	2100–2400	120	13 / 7	B
ERIN18	UT Austin	1280–1600	114–137	18 / 12	B
VERM14	Shell	581–1072	9–300	8 / 5	A
JIN20	UT Austin	143–4400	4.5–9.6	22 / 11	A, B
CLARKE16	Schlumberger	435–465	34	2 / 1	A
IRFAN21	UTP	1750	34	4 / 1	A
EHREN13	UT Austin	169–2906	149–300	26 / 12	A, B

Appendix B. Evidence-unit classification and reasons

Classification rule. Each evidence unit is assigned exactly one of four labels by the following hierarchy, applied in order. First, does the unit contain or preserve an interpretable observation bearing on polymer elasticity, residual-oil displacement, porous-medium resistance or field accessibility? If not, it is Excluded. Second, does it satisfy the full matched-reference admission criteria of Section 2.1? If so, it is Admitted. Third, can the observation still inform interpretation, risk of bias, carbonate applicability, mode contrast or experimental design without entering pooled or cell statistics? If so, it is Supportive; if not, it is Excluded. A unit reporting the same experiments as a more complete source is labelled a Merged duplicate and is never counted twice. Step three is applied with a positive test. A unit is Supportive only where at least one numerically extractable quantity bearing on the question can be recovered from the source: an endpoint saturation, an in-situ resistance measurement, or a mode contrast on a stated saturation basis. Otherwise it is Excluded.

Supportive units carry original or recoverable experimental evidence that informs at least one component of the question but fail one or more admission requirements: no lower-elasticity or Newtonian reference, cross-core comparison without adequate matching, simultaneous viscosity and elasticity differences, recovery reported without a defensible endpoint saturation, missing interfacial tension, geometry, velocity basis or pressure-gradient information, inadequate stage-level provenance, or salinity, sequence and displacement-history confounding. They inform the Discussion, the domain-resolved assessment, the search-gap statement and the proposed experiment, and contribute to no pooled or cell statistic.

Excluded units cannot provide interpretable evidence for the residual-oil-desaturation question even qualitatively: reviews without uniquely recoverable primary data, theory-only or simulation-only studies, bulk-rheology-only studies, single-phase tests without bearing on the carbonate onset analysis, field-only reports without interpretable laboratory displacement evidence, formulations in which interfacial-tension reduction dominates and no polymer-mechanism contrast can be extracted, and sources whose reported information is too incomplete to establish what fluids, sequence, saturation basis or comparison was used.

Same-study merges (five). The Erincik 2017 conference paper and the 2018 SPE Journal paper are one study; the Koh 2015 dissertation and Koh et al. 2018 are one study; the Wang Demin 2000 and 2001 papers and SPE-68723 are one Daqing study (two merges); and the Laudon 2024 conference paper reports the same Indiana limestone corefloods as the 2026 journal article, which supersedes it. Experiments 7–12 and 19 of the Azad and Trivedi (2021) compilation are the Ehrenfried (2013) and Cottin et al. (2014) floods and were extracted from the original full texts, so the compilation contributes no unit of its own.

Zeynalli et al. (2023); Azad and Trivedi (2019): Excluded. Reviews; no primary coreflood data.

Azad and Trivedi (2021): Excluded. Compilation of other groups' floods; used as convention and verification source. Its compiled points enter only through the original papers to avoid double counting.

Qi et al. (2018, EDC); Guo et al. (2022): Excluded. Simulation model and convention review; no new experimental S_{or}.

Chatzis and Morrow (1984); Abrams (1975); Humphry et al. (2014): Excluded. Newtonian contextual anchors. Abrams and Chatzis-Morrow are retained outside the viscoelastic evidence tiers to define the conventional capillary-desaturation benchmark; Humphry et al. carry wettability-resolved Newtonian desaturation context. They carry no evidence on the incremental effect of polymer elasticity.

Seright 2011 (inventoried, not cited); Seright and Wang (2023); Seright et al. (2023): Excluded. Rheology and reviews; no matched-reference S_{or} floods.

Wang et al. (2008a); Wang et al. (2008b); Azad and Seright (2025); Fabbri et al. (2021): Excluded. Field analyses and design studies; Fabbri reports no S_{or}-reduction measurement and is used for carbonate context only. Masalmeh et al. (2019) and Alfazazi et al. (2021) are cited for carbonate in-situ-rheology context in Section 3.6 and are likewise Excluded as evidence units (no matched-reference S_{or} floods).

Koh 2015 dissertation; Erincik 2017 conference: Merged duplicate. Same studies as Koh et al. 2018 and Erincik et al. 2018; merged, never double-counted.

Wang et al. (2000, 2001a, 2001b): Merged duplicate, Supportive. One Daqing study; Supportive because saturations are recovery-basis and IFT/geometry are unreported.

Huh and Pope (2008) secondary set (Wreath, 1989, thesis): Supportive. Underlying thesis data (Wreath, 1989; a companion 1995 thesis not obtained) not yet in hand; carried as Supportive digitized points. Wreath is counted within this unit, not as a fortieth document.

Koh et al. (2018); Barri et al. (2023); Jiang et al. (2008); Sandengen et al. (2017); Du et al. (2021): Supportive. Supportive: no inelastic reference, missing IFT, figure-grade, or chip-scale. The Jiang study includes a glycerol comparison (their Fig. 6); it remains Supportive on data grade and unreported interfacial tension.

Laudon et al. 2024 (SPE-218150-MS): Merged duplicate. Reports the same five Indiana limestone corefloods as Laudon et al. 2026; the journal version additionally carries the 90 °C series. Counted once, through the 2026 source.

Dafaalla et al. 2025; Jain et al. 2026: Supportive. Carbonate polymer contrasts that differ simultaneously in viscosity and elasticity and are run across separate cores, so elasticity is not isolable; Jain reports no endpoint saturation.

Dhahir et al. 2026 (SPE-231553-MS): Supportive. Carbonate capillary-desaturation curves at high salinity and 95 °C. The preceding glycerol stage is a bypassed-oil sweep at a single flux by the authors' own statement, not a matched inelastic reference, and salinity is the deliberate variable, so no contrast holds it constant. The closest near-miss in the screened record.

Jameel et al. 2026 (SPE-231475-MS): Excluded. Bentheimer sandstone; the comparator is a surfactant-glycerol solution whose interfacial tension differs from the polymer by a factor of two, no endpoint saturation is reported for its own corefloods, and no numerically extractable quantity bearing on the question survives the interfacial-tension confound. An earlier Supportive log entry is superseded by the full-text screening.

Laudon et al. 2026: Supportive. Indiana limestone; the viscosity-matched inelastic reference sits in different cores from the elastic fluid, and the authors attribute the additional recovery to lower interfacial tension together with elasticity.

Table B.1. Domain-resolved design and reporting assessment of the seven admitted studies.

Study	**D1**	**D2**	**D3**	**D4**	**D5**	**D6**	**D7**	**D8**	**D9**	**D10**
QI17	M	M	M	L	L	H	U	M	M	M
ERIN18	M	M	M	L	M	M	H	M	H	M
VERM14	M	M	L	M	H	H	U	M	M	H
JIN20	L	M	L	L	M	M	M	M	M	M
CLARKE16	L	U	L	H	L	H	M	L	L	H
IRFAN21	H	U	M	L	U	H	L	H	M	H
EHREN13	H	H	L	M	M	M	M	M	H	H

L low concern, M some concern, H high concern, U unclear. A criterion is rated low concern only where it is satisfied for all admitted contrasts used in the relevant analysis; some concern where it holds for a subset, through an indirect proxy, or with incomplete reporting; high concern where it fails for the contrasts used; and unclear where the source does not provide sufficient information. Where a domain varies within a study the rating reflects contrast coverage rather than a study-wide state: QI17 D2 6/7; ERIN18 D2 6/12 determinable and D5 6/12; VERM14 D2 3/5; JIN20 D2 3/11 determinable, D5 approximately 3/11 and D6 1/11; EHREN13 D6 1/12. Domains: D1 in-situ viscosity matching, D2 pressure-gradient matching, D3 comparator elasticity characterization, D4 same-core versus cross-core design, D5 salinity matching, D6 sequence and order control, D7 throughput matching, D8 saturation-measurement method, D9 comparator reuse and serial dependence, D10 data provenance and measurement uncertainty. No composite score is computed; the ten domains are not commensurable.

Supplementary material

S1. Extensional capillary number: replot and implementation verification

The extensional capillary number N_{ce} is prior art (Azad and Trivedi 2021, SPE-204212-PA; US Patent 11,761,331). It is applied here unchanged. The reimplementation reproduces the source pore-scale viscosities to better than 0.4% on each source's own velocity-reporting convention (superficial flux for Darcy-reporting sources, interstitial for frontal-advance reporting), which verifies implementation consistency only. It does not validate the physical model, and it does not establish that N_{ce} resolves the study-level contradiction examined in the main text.

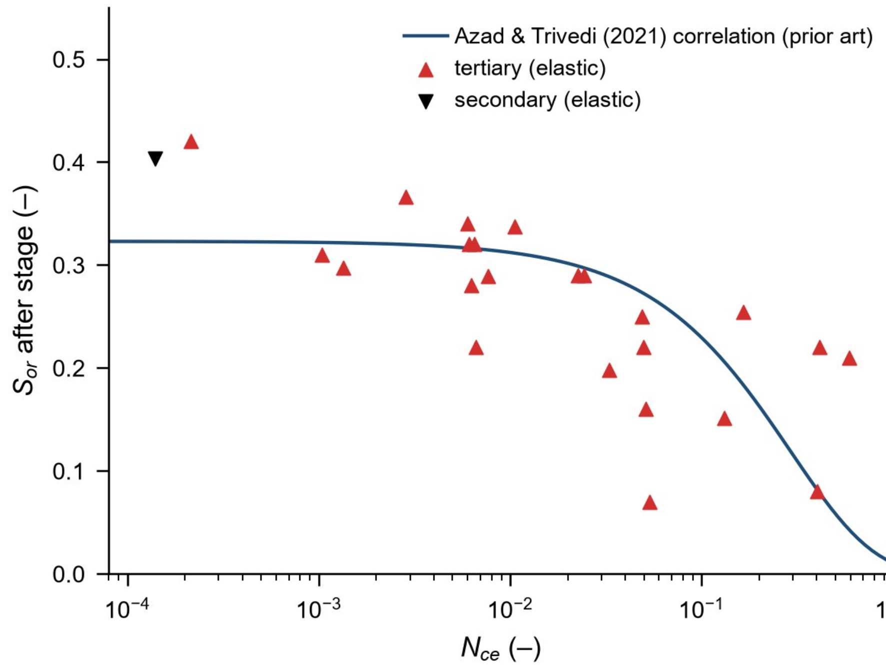

Fig. S1. Admitted stages on the extensional capillary number N_{ce} of Azad and Trivedi; their published correlation is overlaid as prior art and no new fit is made. Verified or digitized N_{ce} values only.

S2. Legacy velocity-or-pressure-gradient classification

The classification used in an earlier version of this analysis assigned a comparison to the high-intensity cell when the interstitial velocity exceeded 1 ft/D (0.3048 m/d) or the pressure gradient reached 10 psi/ft (226.2 kPa/m). That definition is retained only as a sensitivity, because the pressure gradient is in part a response to the elastic resistance under test rather than an imposed condition, and because it groups stages that differ in velocity by an order of magnitude. The primary analysis in the main text classifies on interstitial velocity alone. This figure is reproduced so that the earlier grouping remains inspectable.

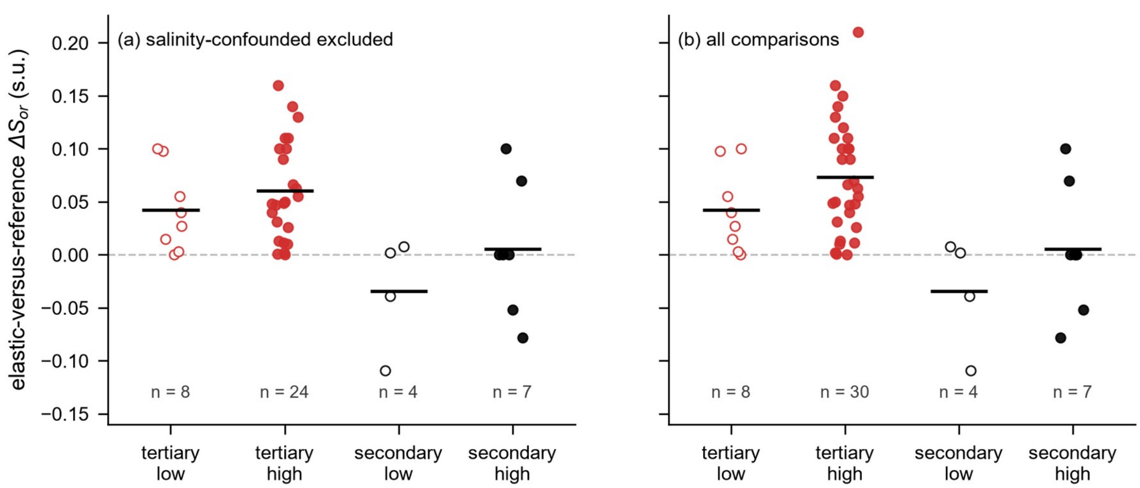

Fig. S2. Elastic-versus-reference ΔS_{or} by injection mode and flow-intensity regime under the legacy velocity-or-pressure-gradient classification: (a) salinity-confounded stages excluded; (b) all comparisons. Horizontal bars are cell means. Retained as a sensitivity display only; the stage-level statistics quoted in the main text are computed on the velocity-only classification.

S3. Reproducible search update

Databases queried: Crossref, OpenAlex and Semantic Scholar. Window: publication date 1 January 2023 to 3 August 2026 inclusive. Cutoff: 3 August 2026. Records were deduplicated by DOI and then against the screened corpus by title and author.

Query strings: (Q1) viscoelastic polymer flooding residual oil saturation coreflood; (Q2) capillary desaturation curve polymer flooding critical capillary number; (Q3) viscoelastic polymer residual oil saturation reduction coreflood elasticity; (Q4) polyethylene oxide HPAM comparison residual oil saturation limestone core.

Screening rule, declared in the search log prior to screening: a record advanced to full-text screening only where the title or abstract indicated a core-scale flooding experiment, residual oil saturation or capillary desaturation as a reported outcome, and a contrast involving polymer elasticity or a matched reference against which such a contrast could be formed. Records failing any of the three were screened out at title and abstract with the reason recorded.

Stated limitations. OnePetro was not queried directly; SPE records were reached only through their Crossref deposits, so SPE material not deposited to Crossref would not appear. Semantic Scholar returned no records for Q3, an empty result whose cause was not established rather than a screened-out result. No hand-search of the reference lists of included studies was performed, and no grey-literature or thesis-repository search was performed beyond the targeted retrieval already recorded. The corpus is therefore described as screened at the stated cutoff under the stated protocol, not as exhaustive.

Outcome. Six published studies were added: Laudon et al. 2024 (merged into the 2026 journal article reporting the same corefloods), Laudon et al. 2026, Dafaalla et al. 2025, Jain et al. 2026, Dhahir et al. 2026 and Jameel et al. 2026. All six were screened against the admission criteria; none qualified for admission. Four retained units entered the Supportive tier; Jameel et al. 2026 was excluded on full-text screening (no numerically extractable quantity bearing on the question survives its interfacial-tension confound). Nine further records were screened out at title and abstract with logged reasons, and three carbonate-CDC methodology records were retrieved and set aside for framing only; per-query retrieval counts are recorded in the project search log. Classifications and reasons are recorded in Appendix B of the main text.

Table S1. Verification of the N_{ce} implementation against Azad and Trivedi (2021), Table 3 (each case evaluated on the source's reported velocity).

Case	μapp,pore reported (cp)	μapp,pore this work (cp)	Nce reported (–)	Nce this work (–)
Exp. 1 (Qi CF1 HPAM, v = 0.96 ft/D)	168,455	168,384	0.0329	0.0330
Exp. 2 (Qi 1800 ppm, v = 0.2 ft/D)	25,504	25,559	0.0010	0.0010
Exp. 3 (Erincik HS3400, v = 4 ft/D)	493,822	493,816	0.4020	0.4028
Exp. 5 (Erincik LS, v = 1 ft/D)	29,728	29,793	0.0061	0.0061

Worked example (Azad and Trivedi 2021, Experiment 2; source inputs). k = 2,100 md, φ = 0.22, σi = 17.3 mN/m, u = 0.2 ft/D as reported (v_i = 0.909 ft/D), 1,800-ppm HPAM (μp0 = 110 cp, λ = 0.1 s, n = 0.6, τext = 0.352 s, μmax = 560,000 cp, n_2 = 3.57). Eq. 3 with C = 6 gives $\dot{\gamma} = 4.98\ s^{-1}$; Eq. 4 gives μapp,pore = 25,559 cp (shear branch 105 cp; strain-hardening branch 25,454 cp) against 25,504 cp reported; Eq. 5 on the reported velocity gives $N_{ce} = 1.04\times10^{-3}$ against 1.0×10^{-3}. The corresponding corpus flood is CF3-HPAM1800-lo. Two source-internal discrepancies are recorded: the source's equations label the shear-rate velocity interstitial while its tabulated cases reproduce on each source's reported velocity (superficial for Qi, interstitial for Erincik), the convention used throughout this work; and the printed correlation uses exp(−3.42 N_{ce}) in the text while the figure annotation prints a base-10 form. The exponential form reproduces the data and is the one plotted in Fig. S1.

Table S2. Velocity-cut sensitivity under the superseded velocity-or-pressure-gradient classifier (secondary and tertiary comparisons pooled; salinity-confounded stages excluded). Retained as a labelled sensitivity only; the primary velocity-only threshold sensitivity is Fig. 4 of the main text.

Velocity cut (ft/D; m/d)	n high	Mean ΔSor high	n low	Mean ΔSor low
0.5 (0.1524)	41	+0.041	2	+0.011
1.0 (0.3048)	31	+0.048	12	+0.017
2.0 (0.6096)	28	+0.056	15	+0.009

S4/S5. Deposited dataset. The supplementary dataset is deposited in two tables: Table S4 (the full 112-row per-stage dataset with basis tags and per-value provenance; Supportive rows are display-only and enter no statistic) and Table S5 (the 49 elastic-versus-reference contrasts with construction basis, in-core-reference status, injection order, reference grade and ΔN_c flags). The regenerated primary statistics are included with the dataset, with the superseded classifier retained as a labelled block feeding Table S2 and Fig. S2 only.